A Furan Prism Cage: Synthesis, Guest Recognition, and Applications in Constructing Charge-Transfer Cocrystals.

Yongwei Qian†, Shengyang Huang†, Shengwen Li†, Zhenzhuo, Liu, Yang Liu, Guangcheng Wu, Yingchun Liu, Hua Tang, Jiyong Liu, Bin Sun*, Ming Li and Hao Li(s)*

Supporting Information

Table of Contents

1. Materials and General Methods

All reagents and solvents were purchased from commercial sources and used without further purification. Manipulations were performed under a normal laboratory atmosphere unless otherwise noted. The compound 1,3,5-tri(furan-2-yl) benzene (**5**)[1] were prepared according to the literature procedures. Thin layer chromatography (TLC) and column chromatography were operated using silica gel 60F254 and silica gel 60F (Merck 9385, 0.040 – 0.063 mm), respectively. Nuclear magnetic resonance (NMR) spectra were recorded on Bruker AVANCE III 400/500 or Agilent DD2 600 spectrometers, with working frequencies of 400/500/600 MHz for ^{1}H and 100/125/150 MHz for ^{13}C, respectively. Chemical shifts are reported in ppm relative to the residual internal non-deuterated solvent signals ($CDCl_3$: δ = 7.26 ppm,). NOESY spectra were acquired at 298 K with mixing time of 180 ms. ROESY spectra were recorded at 298 K with mixing time of 200 ms. High-resolution mass spectra (HR-MS) were measured on a Fourier transform ion cyclotron resonance mass spectrometry (FT-ICR MS). Maldi-Tof-MS was measured by using Bruker ultraflextreme. Thermal gravimetric analysis was measured by using SDT Q600X-ray crystallographic data were collected using a Bruker D8 Venture diffractometer. The UV-vis spectroscopy was carried by Uv-2600. Fluorescence spectra were measured by using FLS1000. The solid-state spectra were measured by using Shimadzu UV-VIS-NIR (UV3600Plus+UV2700). X-ray Powder Diffraction (XRD) tests were measured by using Bruker D8 Discover. All the DFT calculations were performed with ORCA program. For geometry optimization and frequency analysis we adopted the hybrid functional by using the B3LYP with DFT-D3BJ dispersion correction. During geometry optimization we used the valence triple-ζ basis set def-TZVP for all atoms. To refine the computed orbital energy, single point calculations were performed using the range-separated hybrid functional ωB97M-V and the def2-TZVPP basis set. Electrostatic potential figures were generated using Multiwfn to produce cube files and visualized with VMDS[2].

2. Synthetic Procedures.

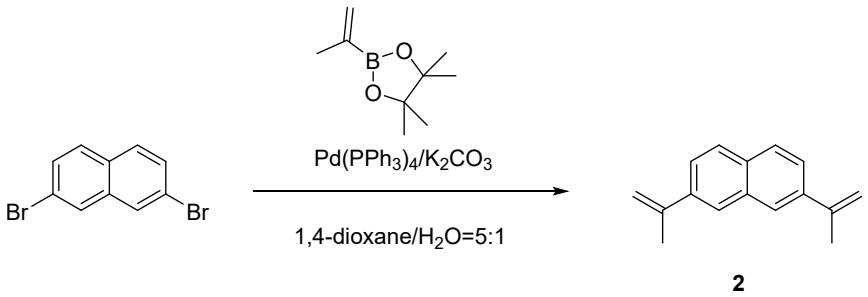

Scheme S1. Synthesis of compound **2.**

2,7-Dibromonaphthalene (1.0 g, 1.0 equiv), isopropenylboronic acid pinacol ester (1.4 g, 2.2 equiv), and K_2CO_3 (2.4 g, 5.0 equiv) were dissolved in 1,4-dioxane (30 mL) and H_2O (6 mL) in a 100 mL three-neck round-bottom flask. After degassed with N_2 three times, tetrakis(triphenylphosphine) palladium (0.2 g, 0.05 equiv) was added under N_2, and then the mixture was heated at 85 °C under N_2 overnight. Upon completion (monitored by TLC, at 16 h), the mixture was cooled, quenched with H_2O (50 mL), and extracted with EtOAc (3 × 20 mL). The combined organic layers were dried through anhydrous Na_2SO_4 and concentrated under reduced pressure. Purification by column chromatography (EtOAc / petroleum ether = 1 / 100, v/v) afforded compound **2** as a white solid (0.65 g, 89 %). ^{1}H NMR （400 MHz, $CDCl_3$）: δ 7.87 (d, *J* = 1.8 Hz, 2H), 7.77 (d, *J* = 8.6 Hz, 2H), 7.66 (dd, *J* = 8.5, 1.8 Hz, 2H), 5.55 (s, 2H), 5.21 (s, 2H), 2.29 (s, 6H). ^{13}C NMR (100 MHz, $CDCl_3$) : δ 145.2, 142.5, 136.5, 130.1, 125.5, 114.6, 21.7. HR-MS-ESI: calculated: 208.1252; found: $[M+H]^+$ 209.1322.

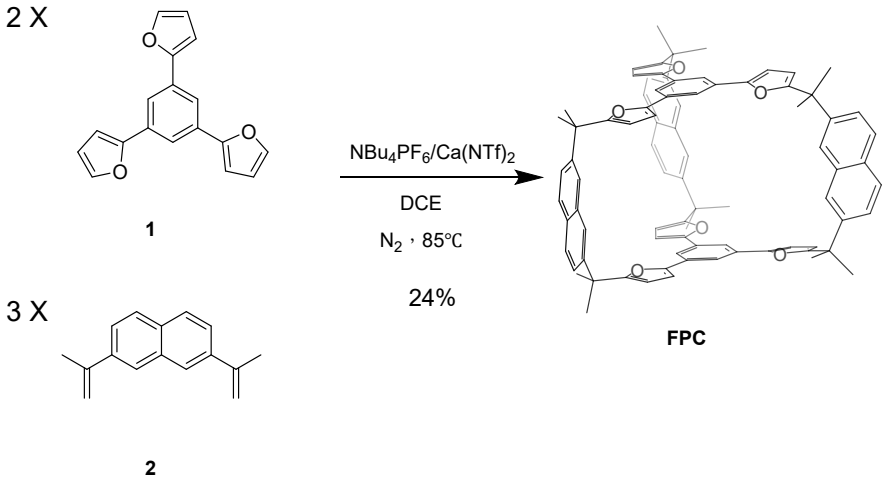

Scheme S2. Synthesis of **FPC.**

2,7-Diisopropenylnaphthalene (**2**, 250 mg, 1.6 equiv), 1,3,5-tris(2-furyl) benzene (**1**, 200 mg, 1.0 equiv), tetrabutylammonium hexafluorophosphate (70 mg, 0.25 equiv), and calcium bis(trifluoromethanesulfonyl)imide (108 mg, 0.25 equiv) were dissolved in 1,2-dichloroethane (50 mL) in a 100 mL two-neck round-bottom flask. The reaction mixture was degassed with N_2 (three cycles), and then heated at 85 °C in an oil bath overnight. After completion (monitored by TLC), the mixture was cooled to room temperature, quenched with H_2O (50 mL), and extracted with CH_2Cl_2 (3 × 40 mL). The combined organic layers were dried over anhydrous Na_2SO_4, filtered, and

concentrated under reduced pressure. The crude product was purified by column chromatography to yield the desired compound **FPC** as a white solid (97 mg, 24%). ^{1}H NMR (500 MHz, $CDCl_3$) δ: 7.78 (d, *J* = 8.8 Hz, 6H), 7.58 (d, *J* = 8.7 Hz, 6H), 7.56 (s, 6H), 7.01 (s, 6H), 6.62 (s, 6H), 6.28 (s, 6H), 1.71 (s, 36H). ^{13}C NMR (125 MHz, $CDCl_3$) δ: 161.1, 152.1, 145.9, 133.2, 131.3, 130.6, 127.5, 124.9, 123.1, 116.1, 107.4, 106.0, 40.9, 29.1. HR-MS-ESI:$[M + H]^+$ calcd for $C_{78}H_{61}O_6$: 1177.533; found: 1177.204.

3. Characterization of ligands and cages.

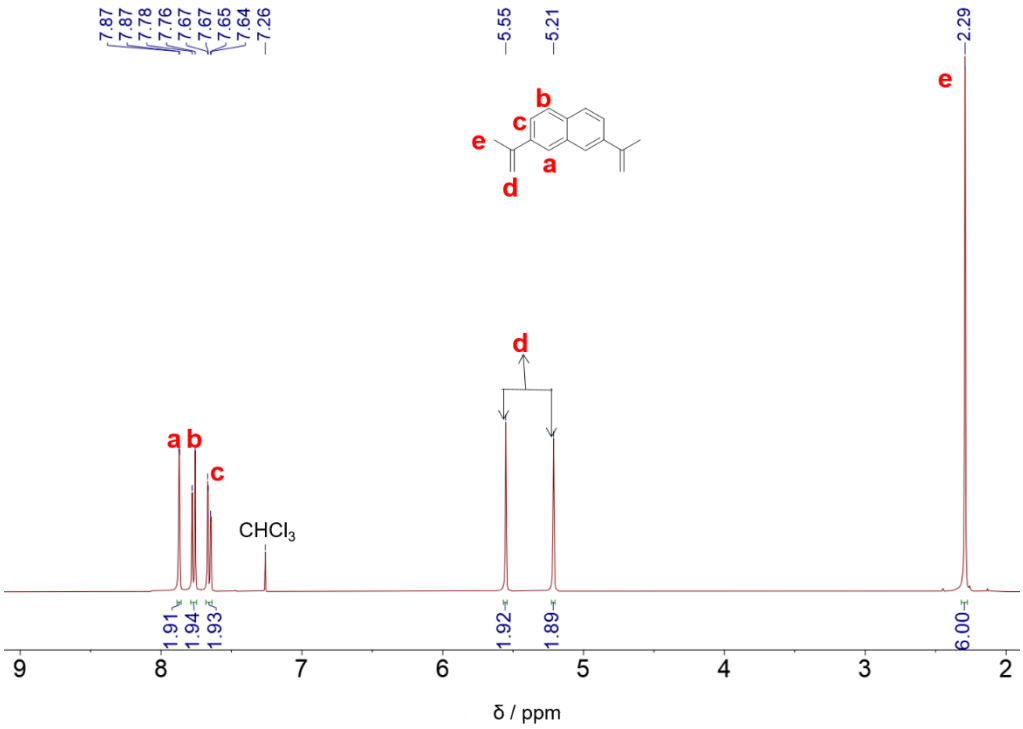

Figure S1. ^{1}H NMR spectrum (600 MHz, $CDCl_3$, 298 K) of **2.**

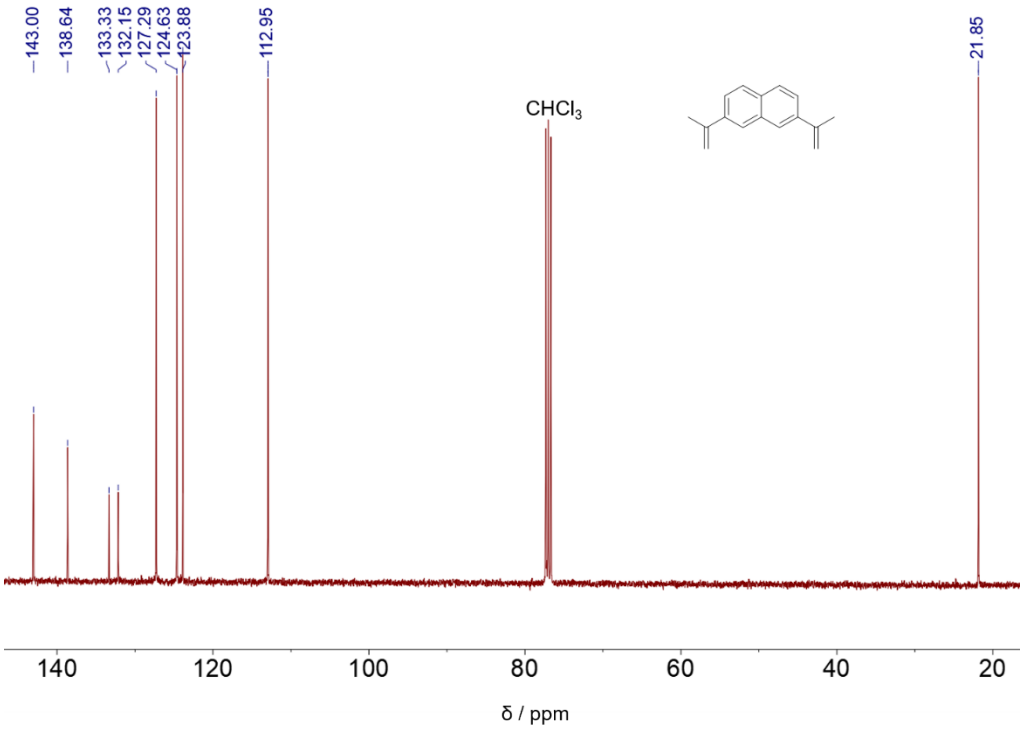

Figure S2. ^{13}C NMR spectrum (150 MHz, $CDCl_3$, 298K) of **2.**

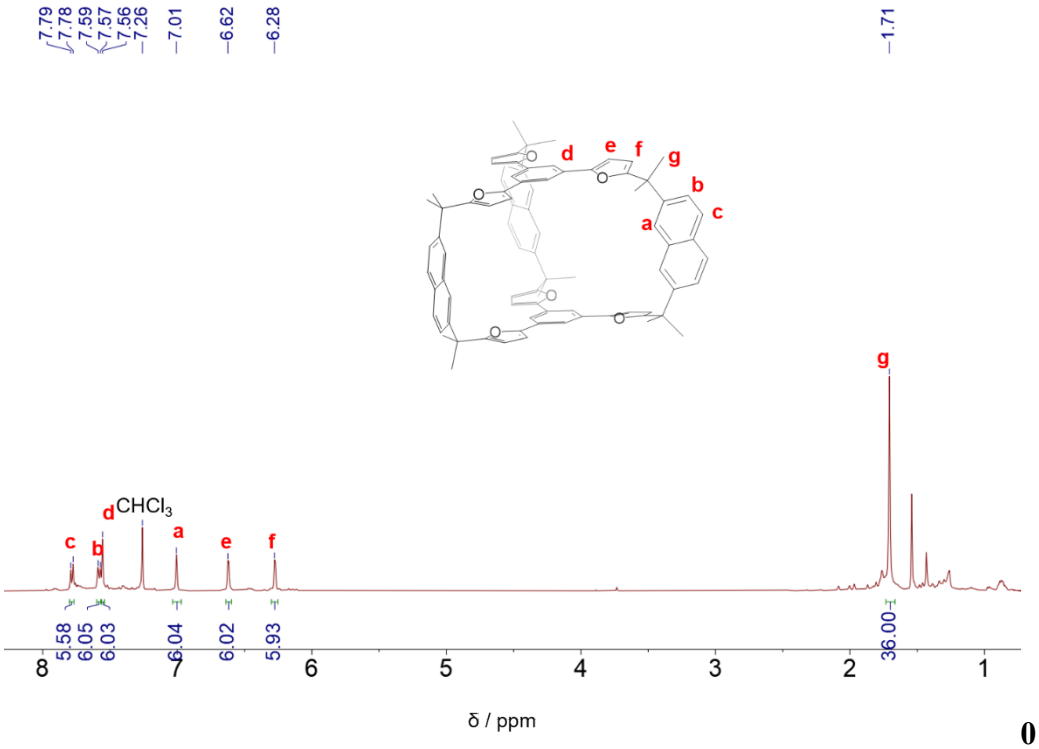

0

Figure S3. ^{1}H NMR spectrum (600 MHz, $CDCl_3$, 298 K) of **FPC.**

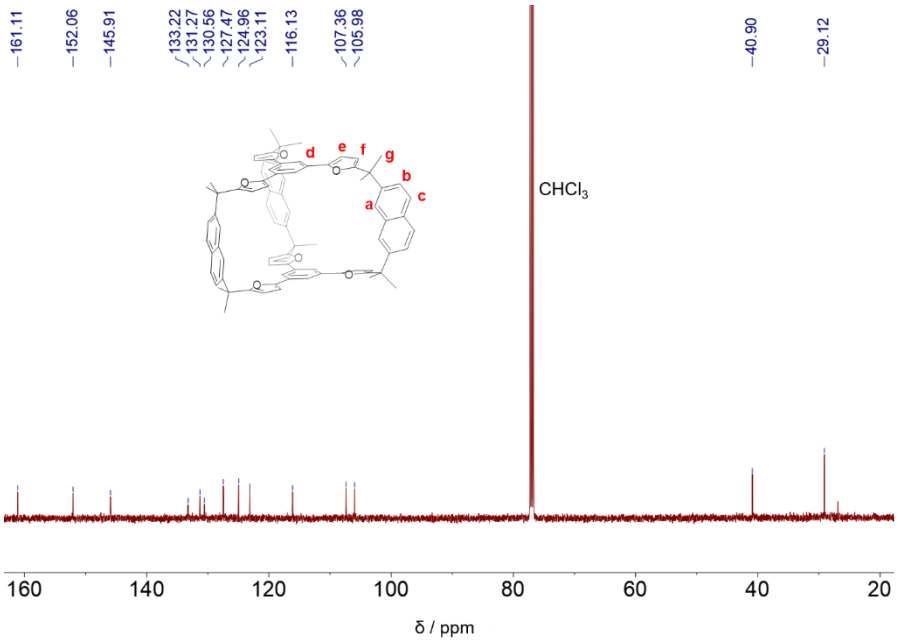

Figure S4. ^{13}C NMR spectrum (150 MHz, $CDCl_3$, 298 K) of **FPC.**

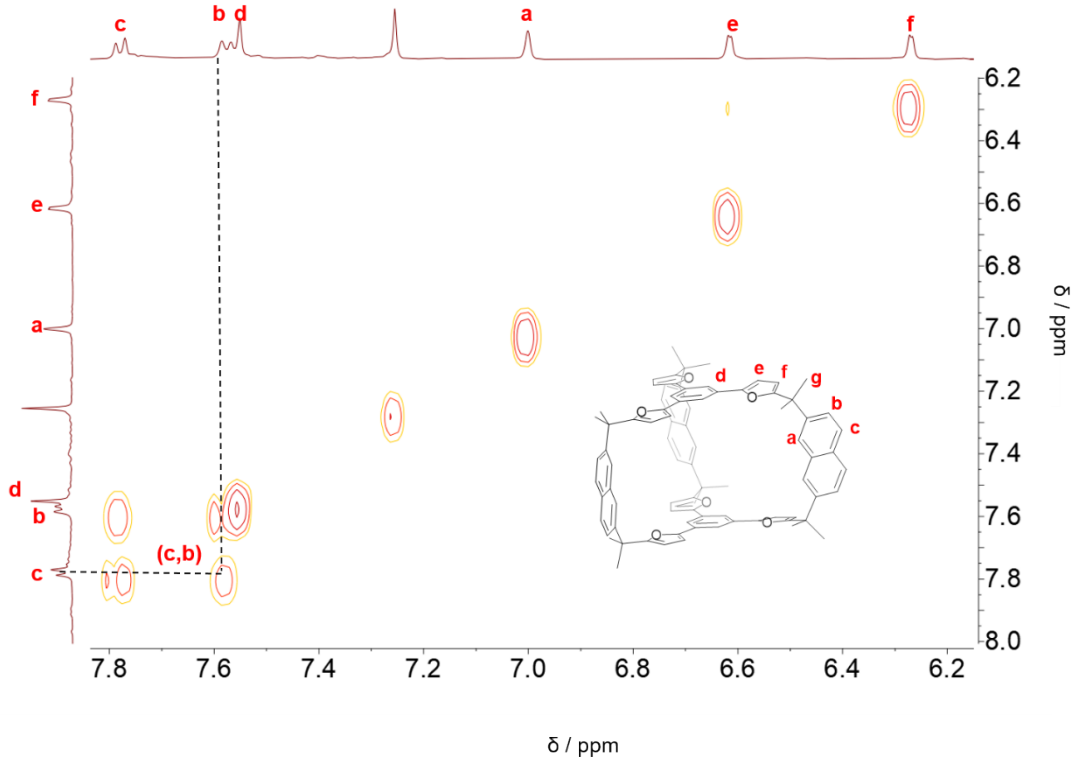

Figure S5. ^{1}H-^{1}H COSY spectrum (600 MHz, $CDCl_3$, 298 K) of **FPC.**

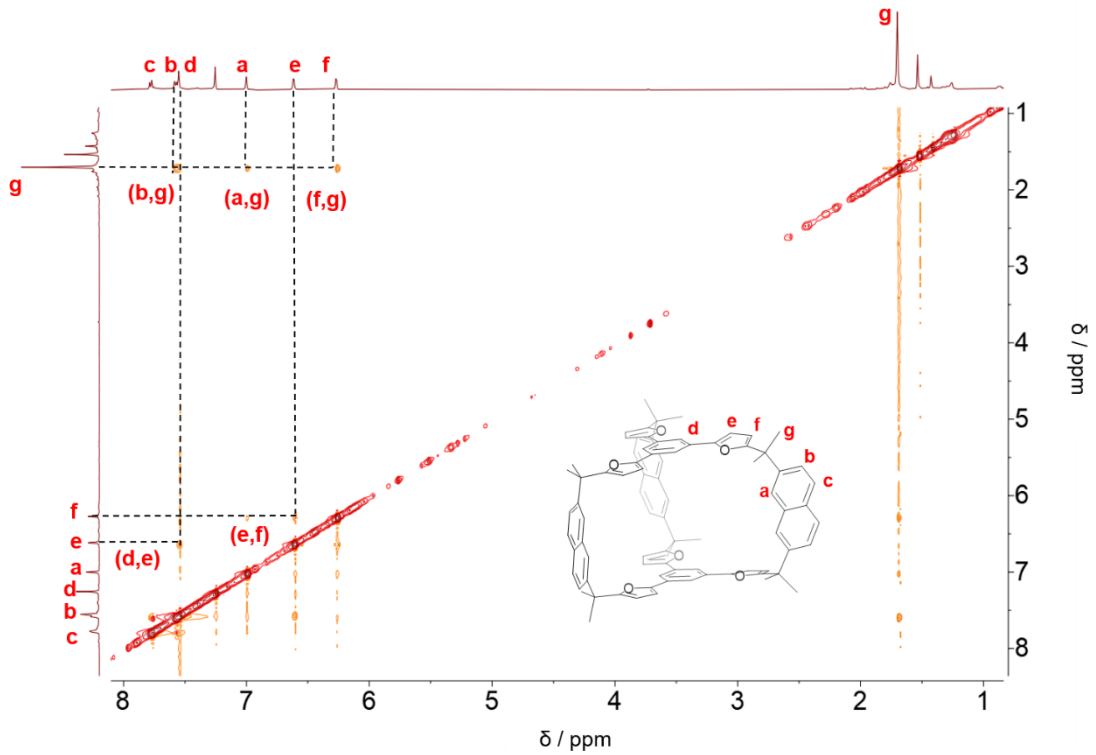

Figure S6. ^{1}H-^{1}H ROESY spectrum (600 MHz, $CDCl_3$, 298K) of **FPC.**

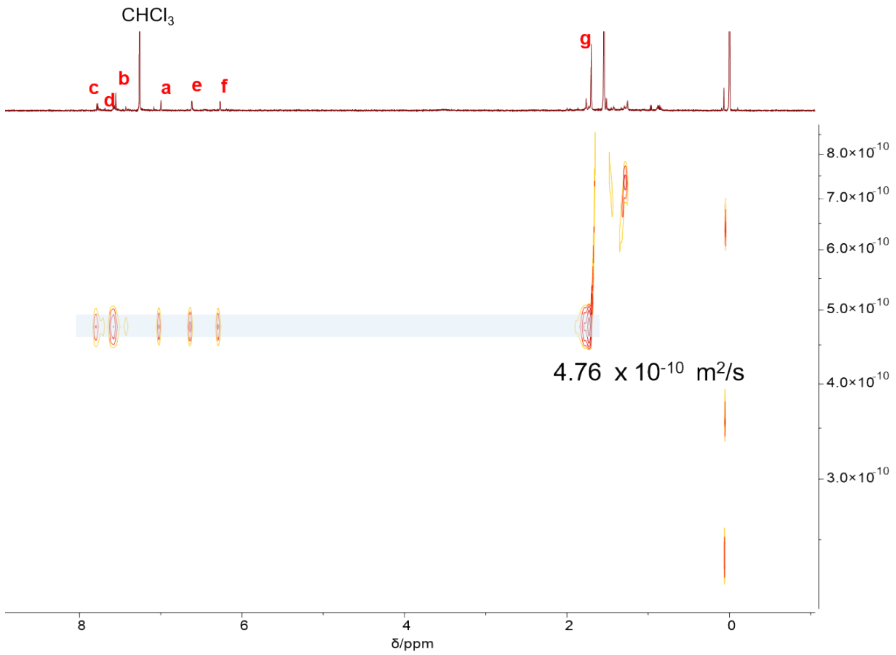

Figure S7. DOSY spectrum of **FPC** (500 MHZ, $CDCl_3$, 298K).

(a)

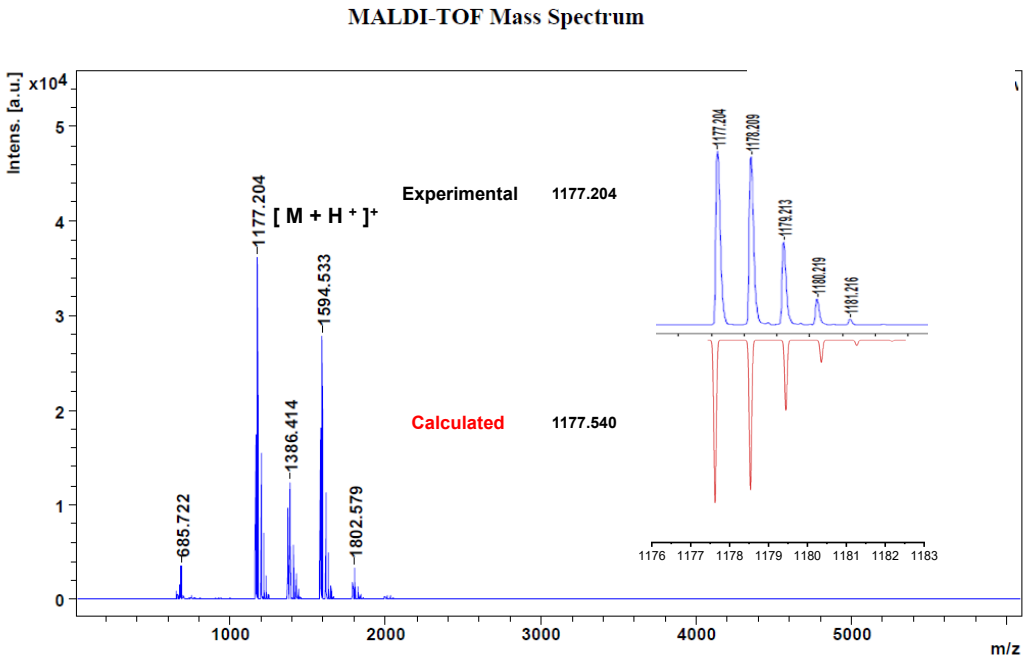

(b)

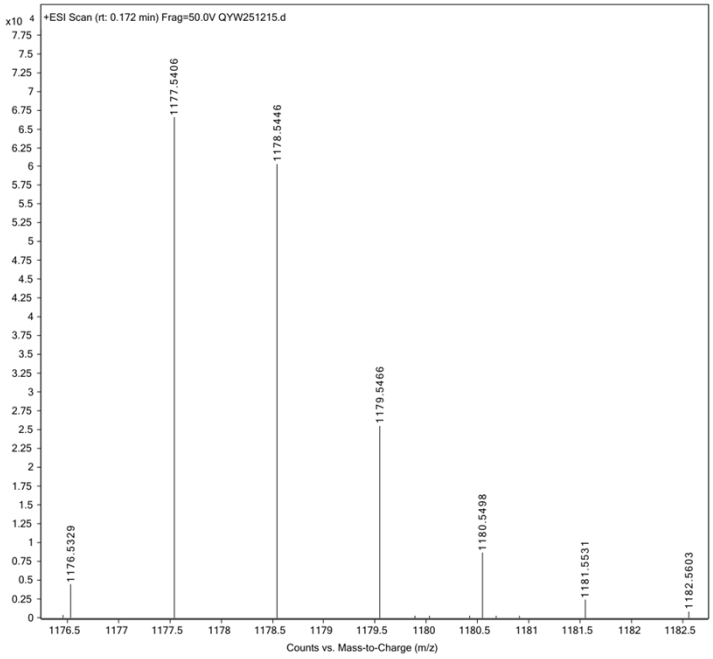

Figure S8. (a) Maldi-Tof-MS spectrum of **FPC.** (b) ESI-MS spectrum of **FPC**.

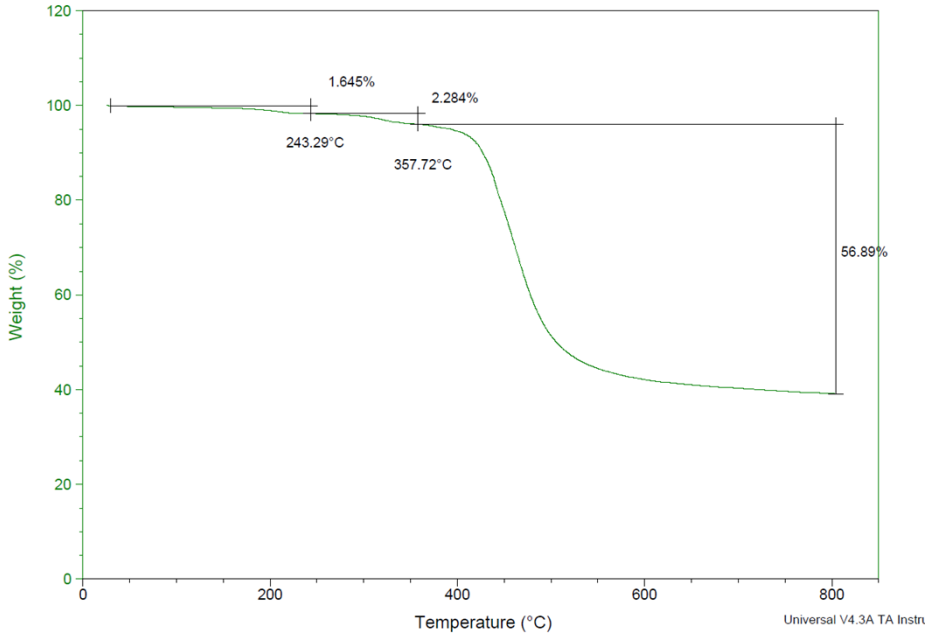

Figure S9. Thermogravimetric analysis of **FPC**.

3. Host-guest recognition studies of FPC.

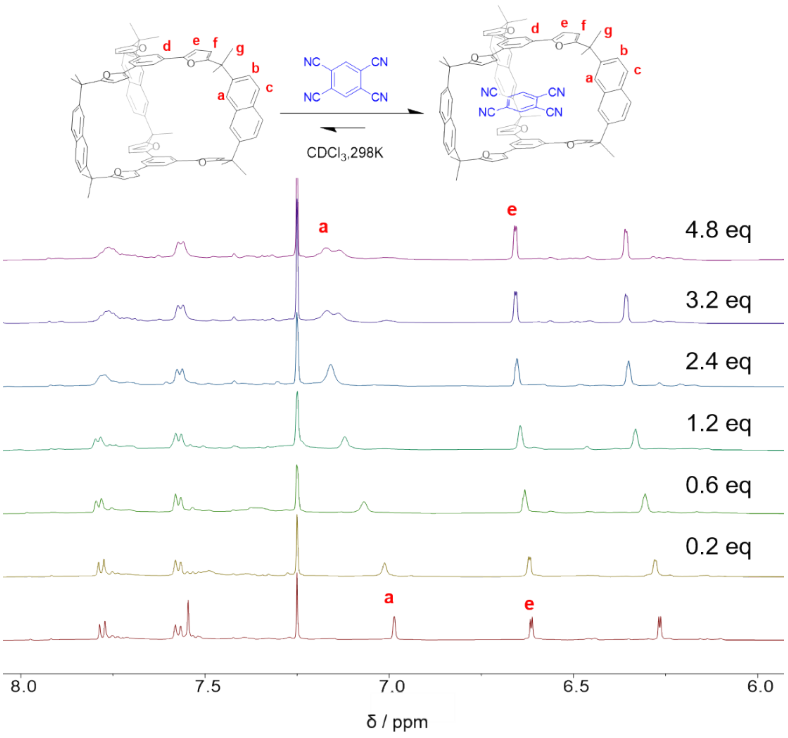

Figure S10. Partial ^{1}H NMR spectra (600 MHz, $CDCl_3$, 298 K) of **FPC** recorded after addition of different amount of **G1** from 0 equiv. (bottom) to 4.8 equiv. (top) with a constant concentration of **FPC** ([C] = 2.8 mM).

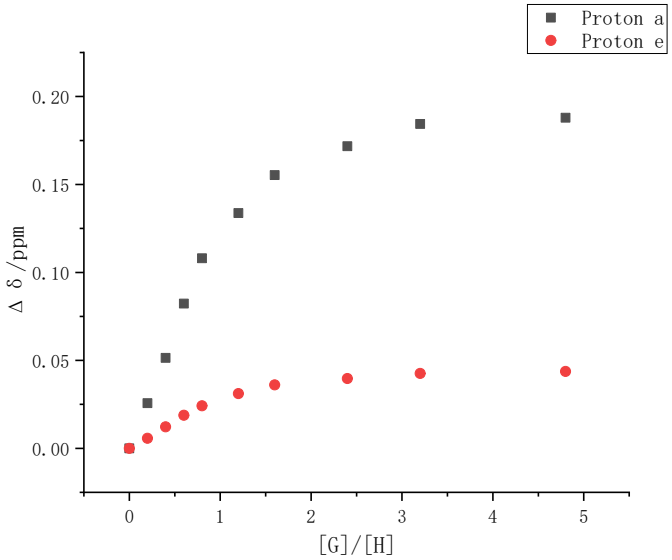

Figure S11. Plots of the chemical shift difference (Δδ) of the protons a (black) and proton e (red) respectively versus the guest-to-host ratio. The data were fitted with 1:1 binding model and gave K_a = (6.0 ± 0.5) × 10^2 M^{-1}.

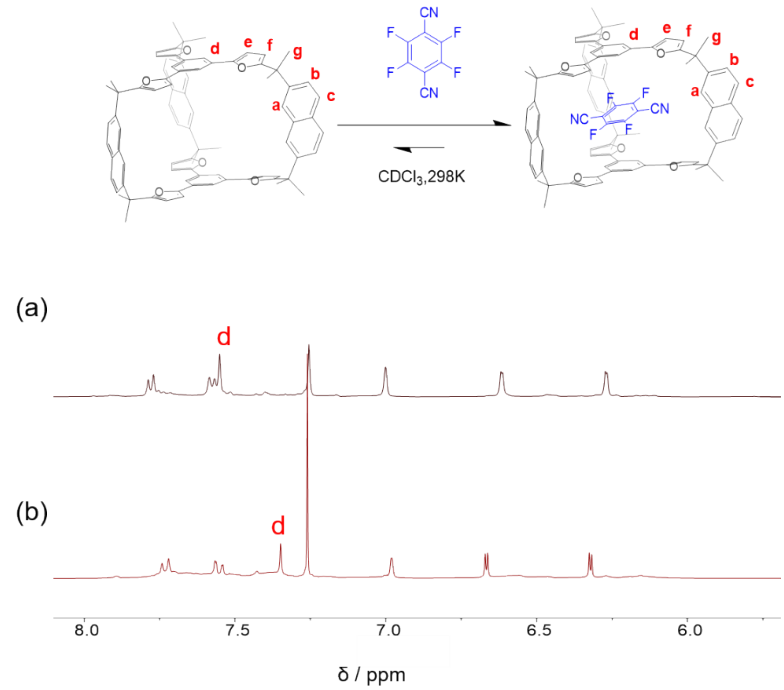

Figure S12. Partial ^{1}H NMR spectra (600 MHz, $CDCl_3$, 298 K) of (a) **FPC** ([C] = 2.8 mM). (b) **FPC** ([C] = 2.8 mM) after addition of two equivalents **G2**.

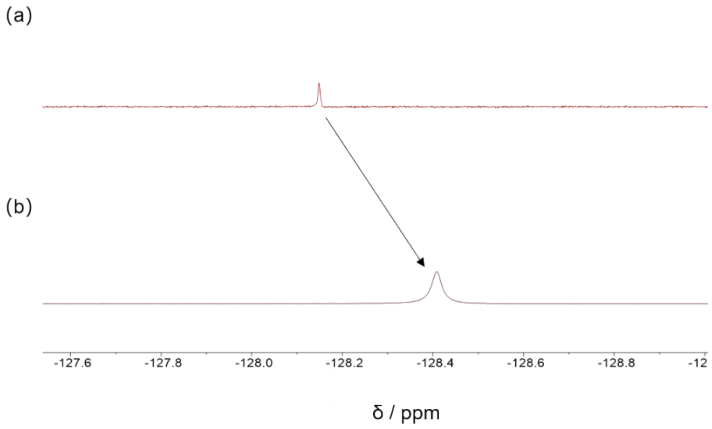

Figure S13. Partial ^{19}F NMR spectra (376 MHz, $CDCl_3$, 298 K) of **FPC** ([C] = 2.8 mM) before (a) and after (b) after addition of two equivalents **G2**.

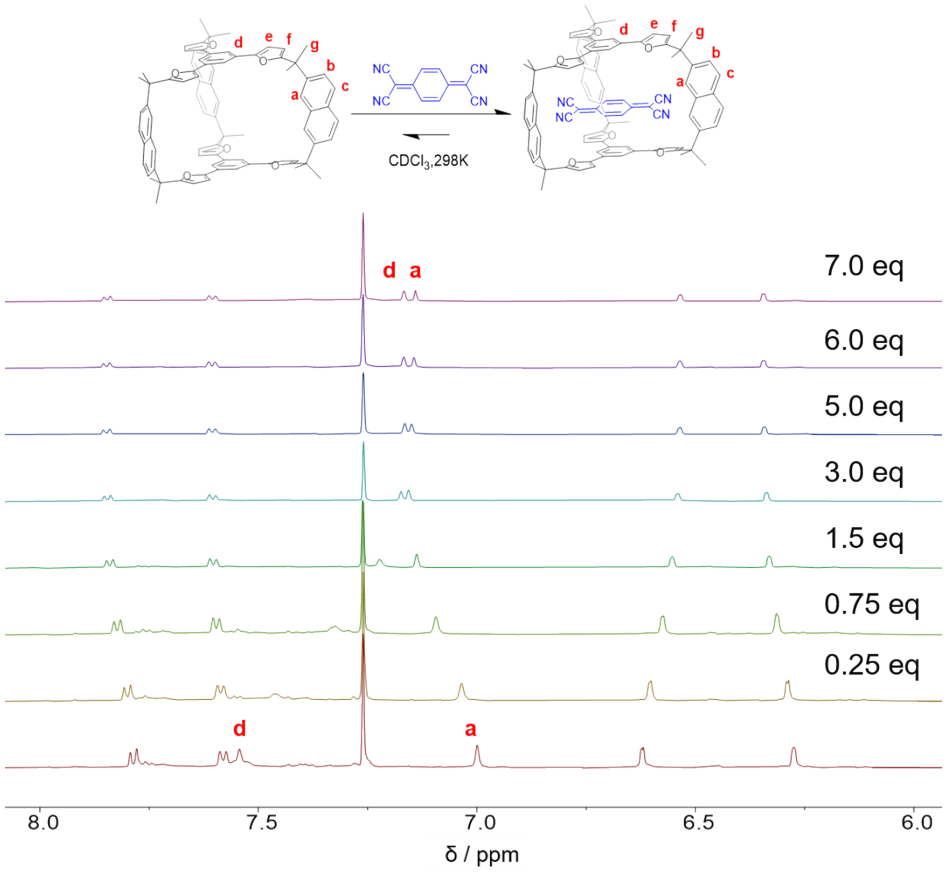

Figure S14. Partial ^{1}H NMR spectra (600 MHz, $CDCl_3$, 298 K) of **FPC** recorded after addition of different amount of **G3** from 0 equiv. (bottom) to 7.0 equiv. (top) with a constant concentration of **FPC** ([C] = 2.8 mM).

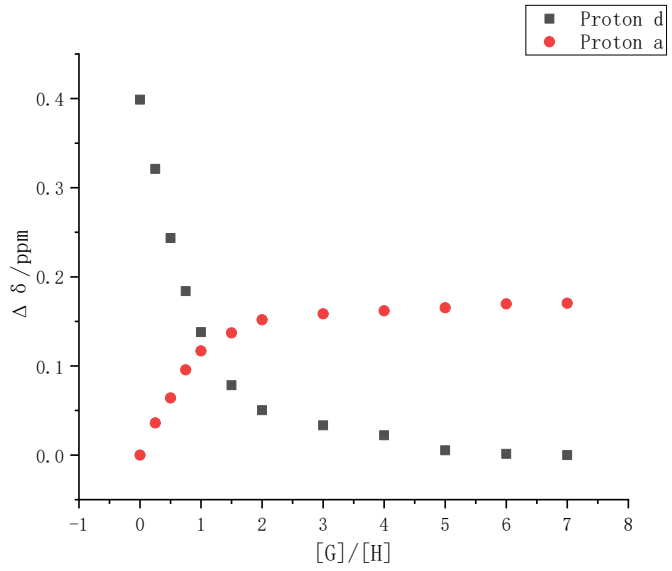

Figure S15. Plots of the chemical shift difference (Δδ) corresponding to the proton d (black) and proton a (red) respectively versus the guest-to-host ratio. The data were fitted with 1:1 binding model and gave $K_a = (1.5 \pm 0.1) \times 10^3$ M^{-1}.

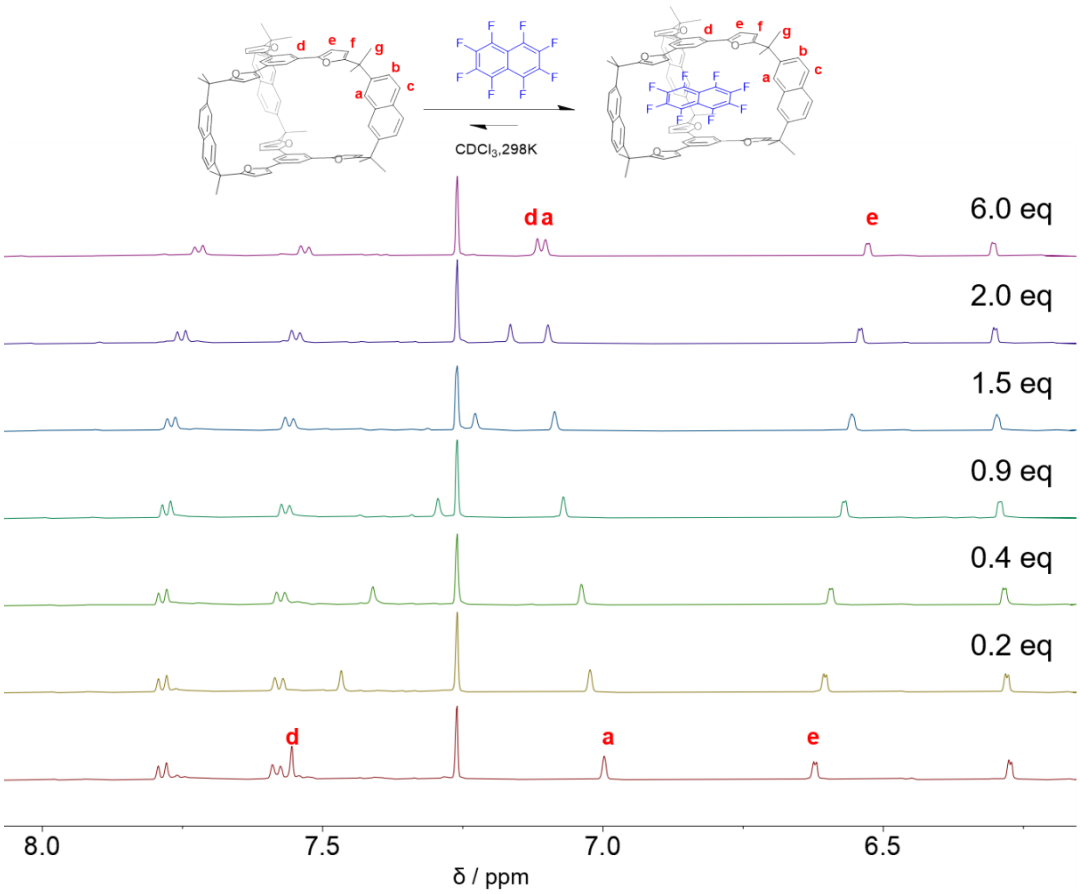

Figure S16. Partial ^{1}H NMR spectra (600 MHz, $CDCl_3$, 298K) of **FPC** recorded after addition of different amount of **G4** from 0 equiv. (bottom) to 6 equiv. (top) with a constant concentration of **FPC** ([C] = 2.8 mM).

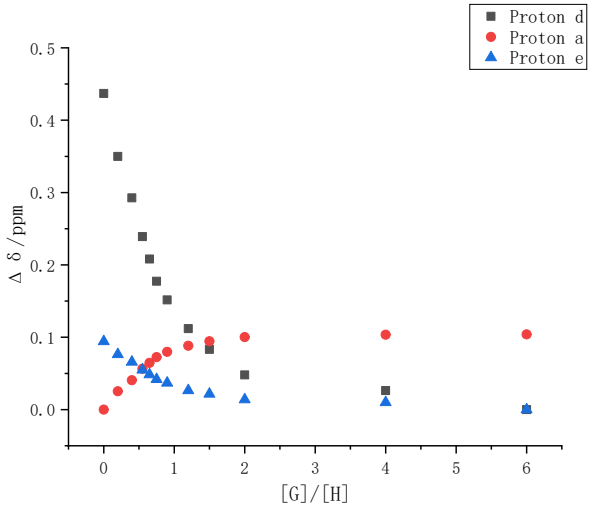

Figure S17. Plots of the chemical shift difference (Δδ) corresponding to proton a (red), proton d (black) and proton e (blue) versus the guest-to-host ratio. The data were fitted with 1:1 binding model and gave $K_a = (2.3 \pm 0.2) \times 10^3$ M^{-1}.

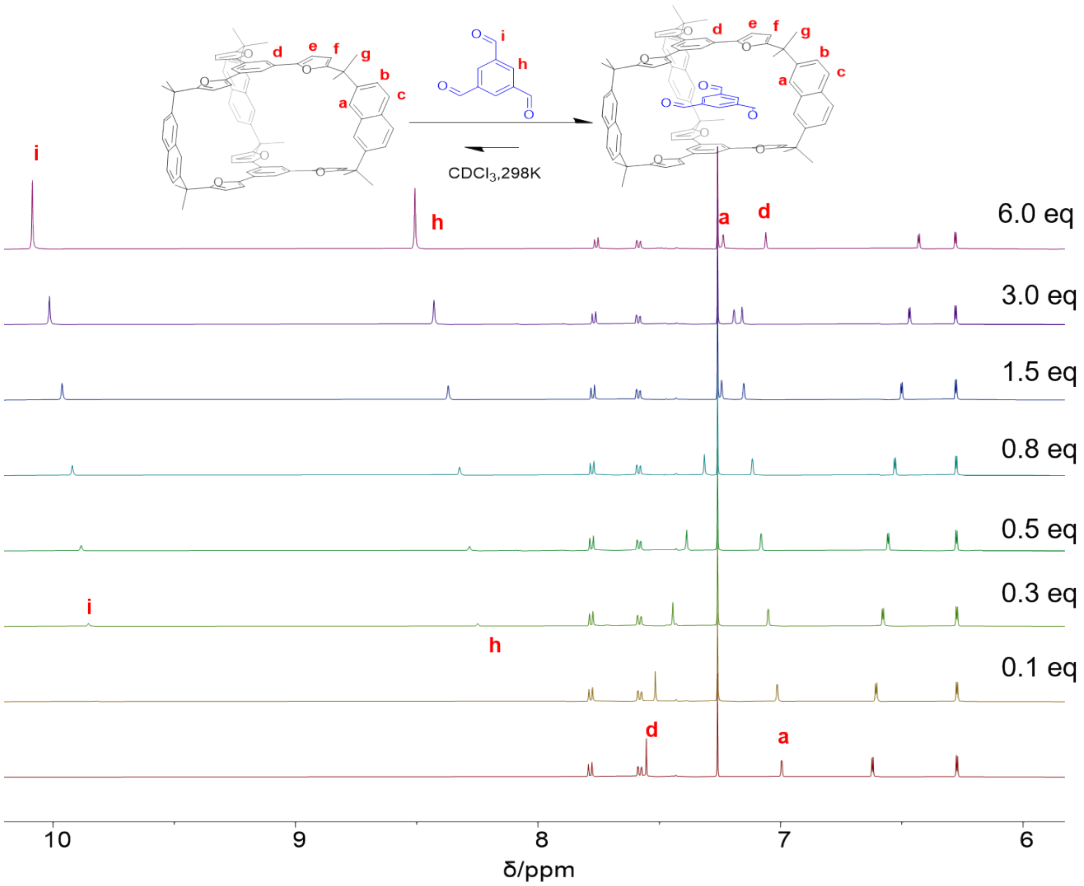

Figure S18. Partial ^{1}H NMR spectra (600 MHz, $CDCl_3$, 298 K) of **FPC** recorded after addition of different amount of **G5** from 0 equiv. (bottom) to 6.0 equiv. (top) with a constant concentration of **FPC** ([C] = 2.8 mM).

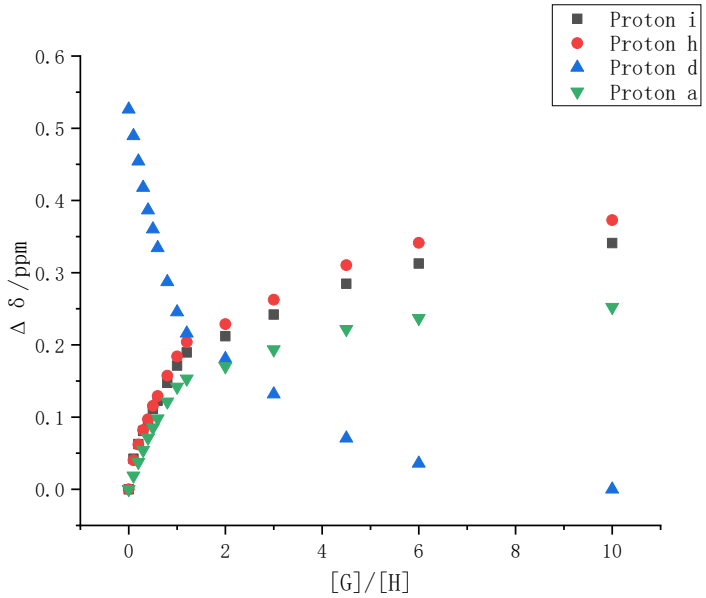

Figure S19. Plots of the chemical shift difference (Δδ) corresponding to the proton i (black), proton h (red), proton d (blue) and proton a (green) versus the host-guest ratio. The data were fitted with 1:1 binding model and gave $K_a = (6.6 \pm 0.6) \times 10^2$ M^{-1}.

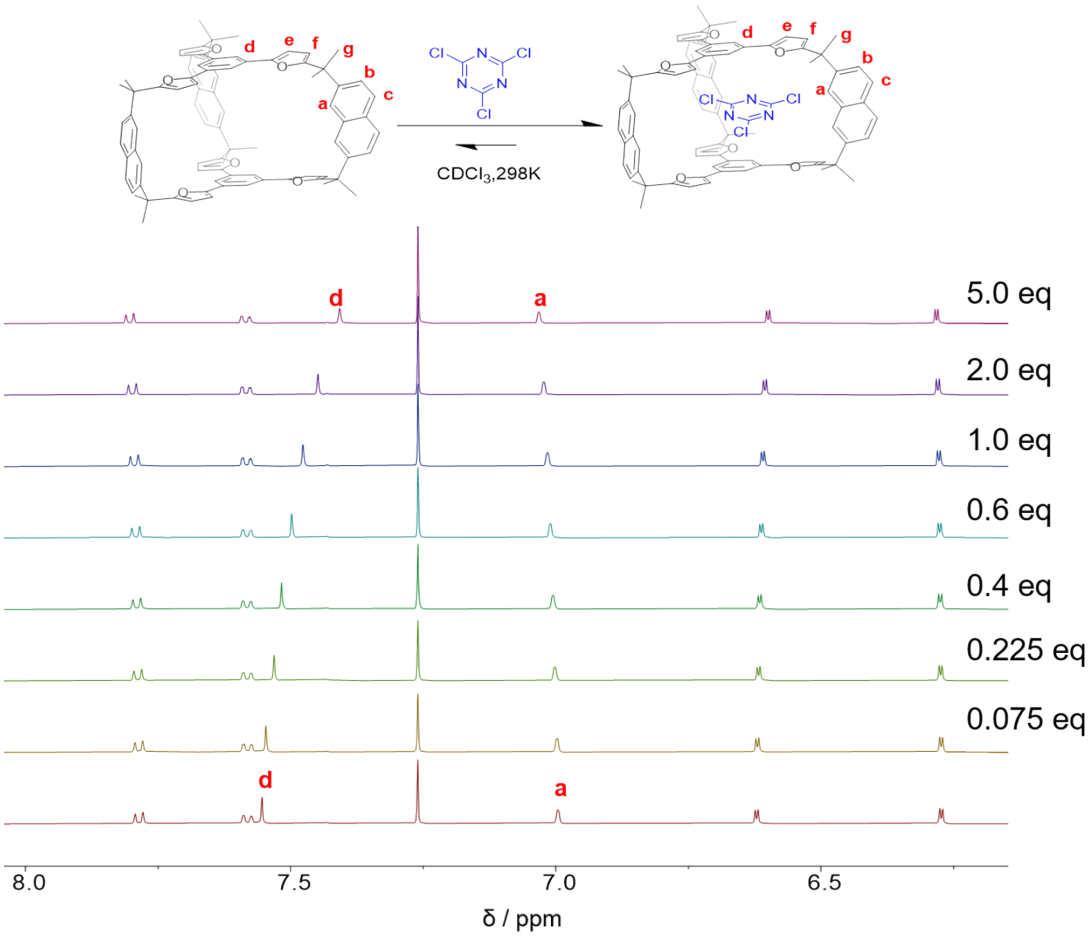

Figure S20. Partial ^{1}H NMR spectra (600 MHz, $CDCl_3$, 298 K) of **FPC** recorded after addition of different amount of **G6** from 0 equiv. (bottom) to 5.0 equiv. (top) with a constant concentration of **FPC** ([C] = 2.8 mM).

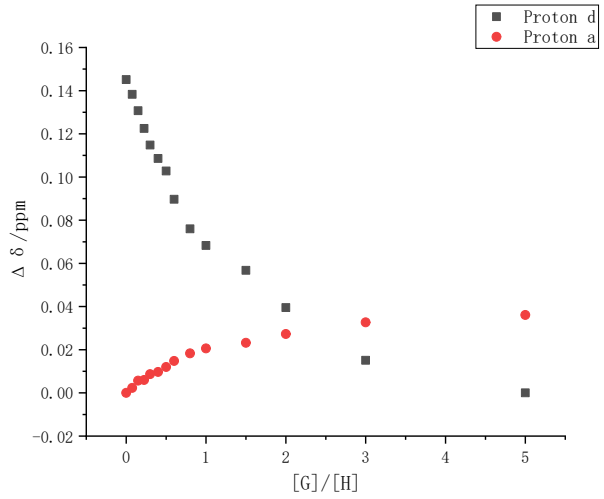

Figure S21. Plots of the chemical shift difference (Δδ) corresponding to the proton a (red) and proton d (black) versus the host-guest ratio. The data were fitted with 1:1 binding model and gave $K_a = (5.0 \pm 0.3) \times 10^2$ M^{-1}.

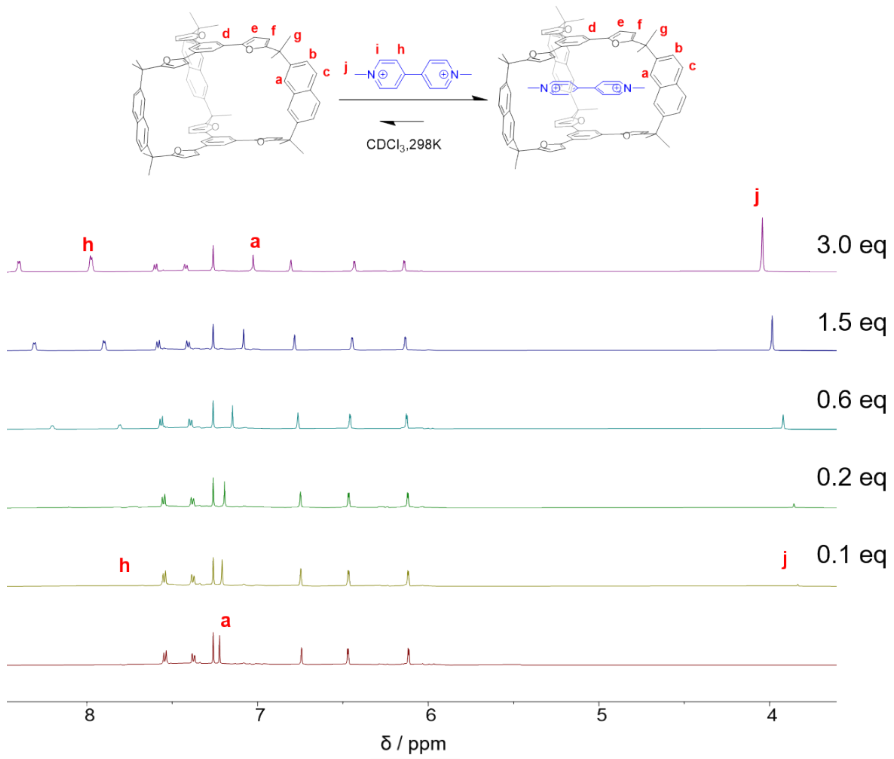

Figure S22. Partial ^{1}H NMR spectra (600 MHz, $CDCl_3/CD_3CN$=1/1, 298 K) of **FPC** recorded after addition of different amount of **G7** from 0 equiv. (bottom) to 3.0 equiv. (top) with a constant concentration of **FPC** ([C] = 2.8 mM).

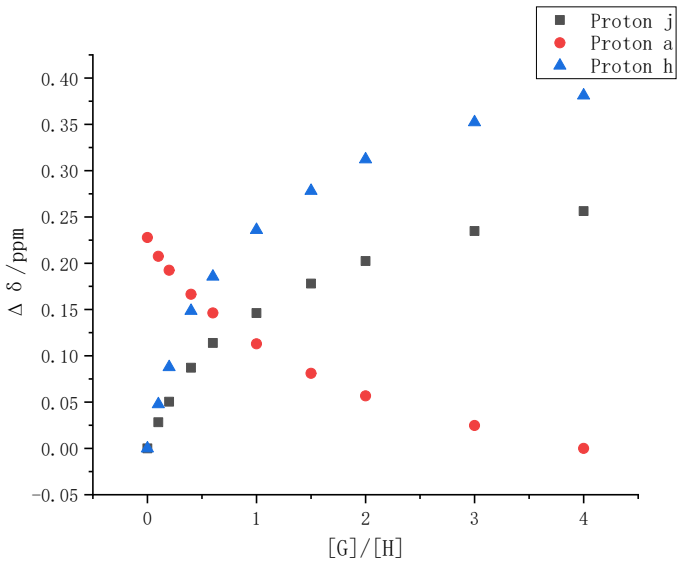

Figure S23. Plots of the chemical shift difference (Δδ) corresponding to proton j (black), proton a (red) and proton h (blue) versus the guest-to-host ratio. The data were fitted with 1:1 binding model and gave $K_a = (5.6 \pm 0.8) \times 10^2$ M^{-1}.

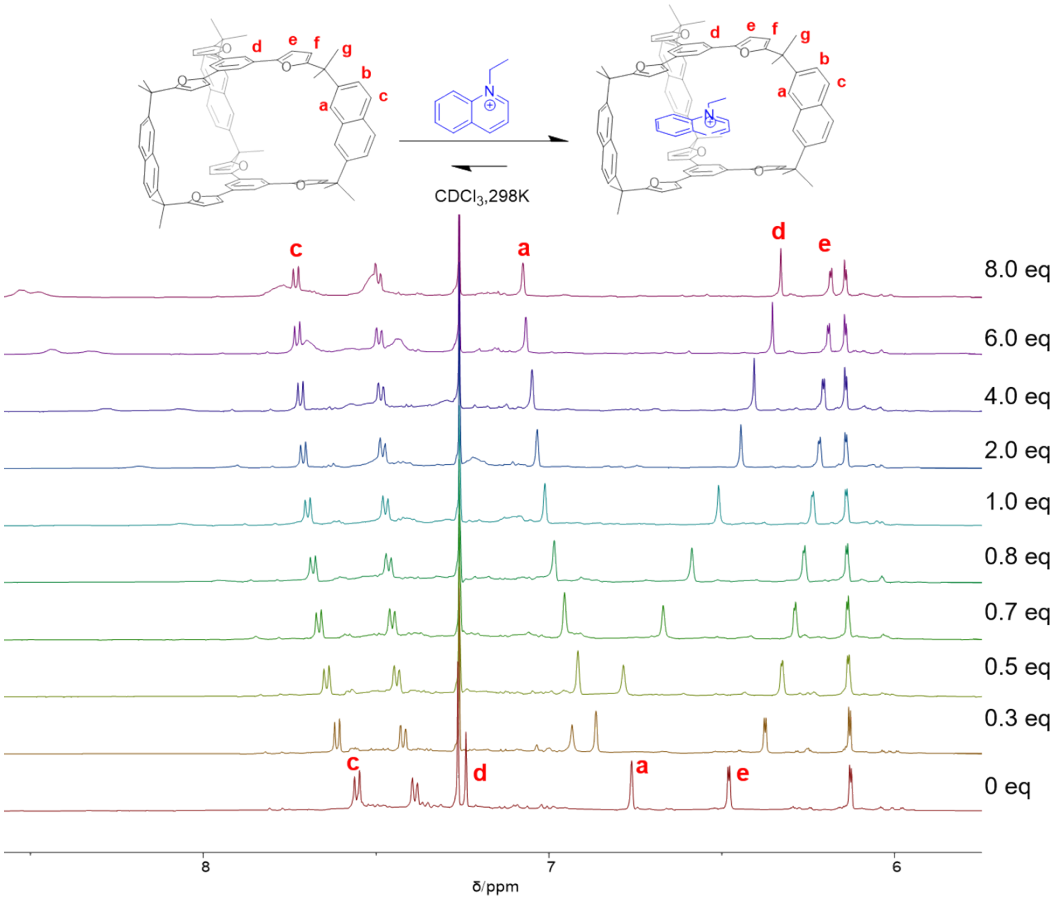

Figure S24. Partial ^{1}H NMR spectra (600 MHz, $CDCl_3$, 298 K) of **FPC**) recorded after addition of different amount of **G8** from 0 equiv. (bottom) to 8.0 equiv. (top) with a constant concentration of **FPC** ([C] = 2.8 mM).

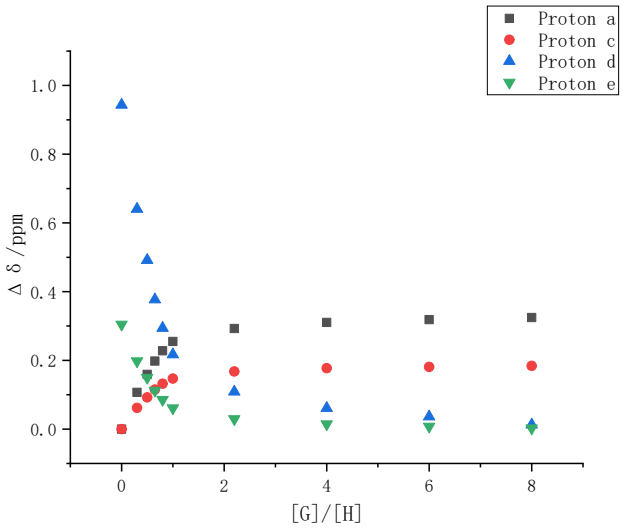

Figure S25. Plots of the chemical shift difference (Δδ) corresponding to the proton a (black), proton c (red), proton d (blue) and proton e (green) versus the guest-to-host ratio. The data were fitted with 1:1 binding model and gave $K_a = (1.0 \pm 0.2) \times 10^4$ M^{-1}.

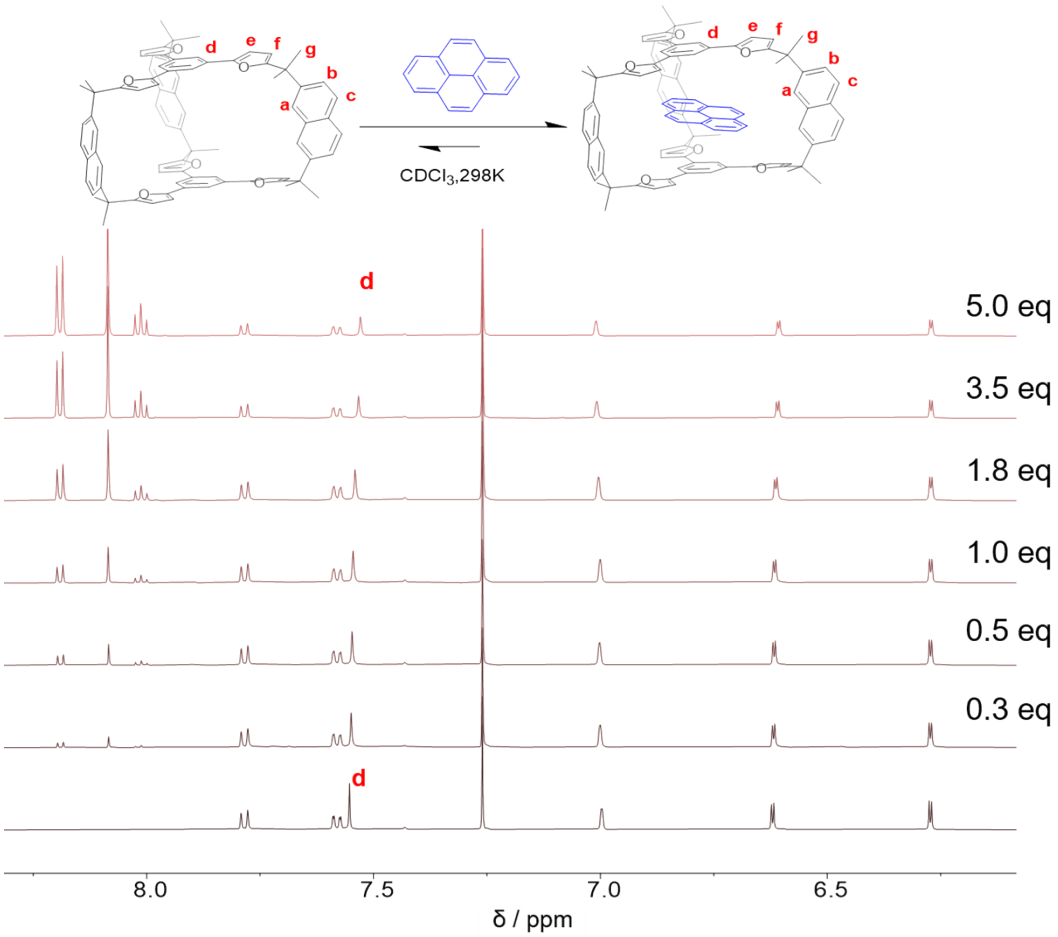

Figure S26. Partial ^{1}H NMR spectra (600 MHz, $CDCl_3$, 298 K) of **FPC** recorded after addition of different amount of **G9** from 0 equiv. (bottom) to 5.0 equiv. (top) with a constant concentration of **FPC** ([C] = 2.8 mM).

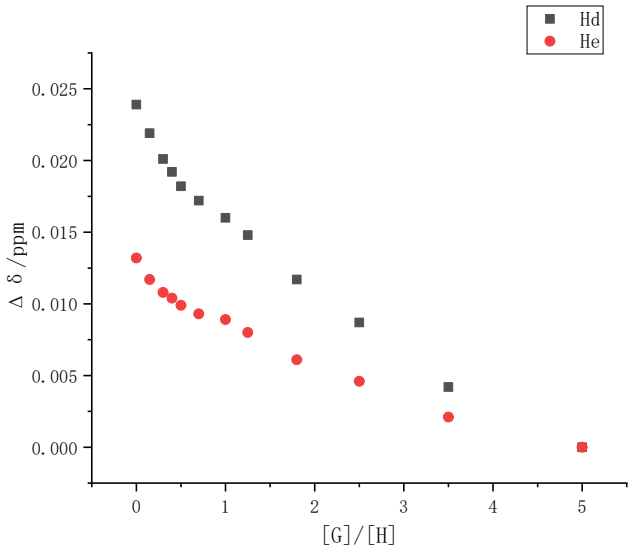

Figure S27. Plots of the chemical shift difference (Δδ) corresponding to the proton e (red) and proton d (black) versus the guest-to-host ratio. The data fitted with 1:1 binding model and gave *K*a = (1.0 ± 0.0) × 10^2 M^{-1}.

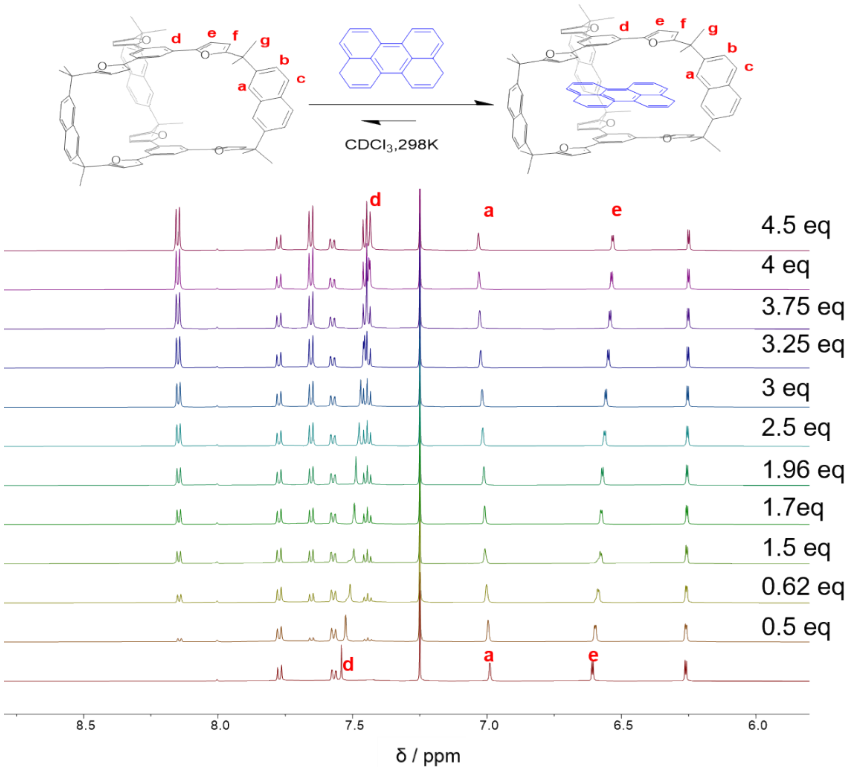

Figure S28. Partial ^{1}H NMR spectra (600 MHz, $CDCl_3$, 298 K) of **FPC** recorded after addition of different amount of **G10** from 0 equiv. (bottom) to 4.5 equiv. (top) with a constant concentration of **FPC** ([C] = 2.8 mM).

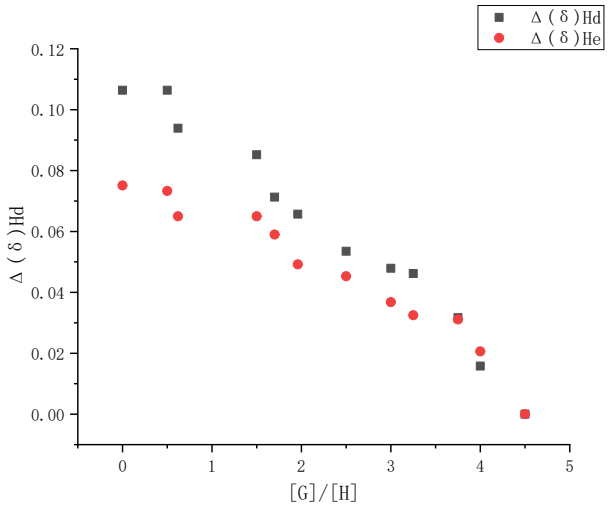

Figure S29. Plots of the chemical shift difference (Δδ) corresponding to the proton e (red) and proton d (black) versus the guest-to-host ratio. The data were fitted with 1:1 binding model and gave $K_a = (3.7 \pm 0.1) \times 10^2\ M^{-1}$.

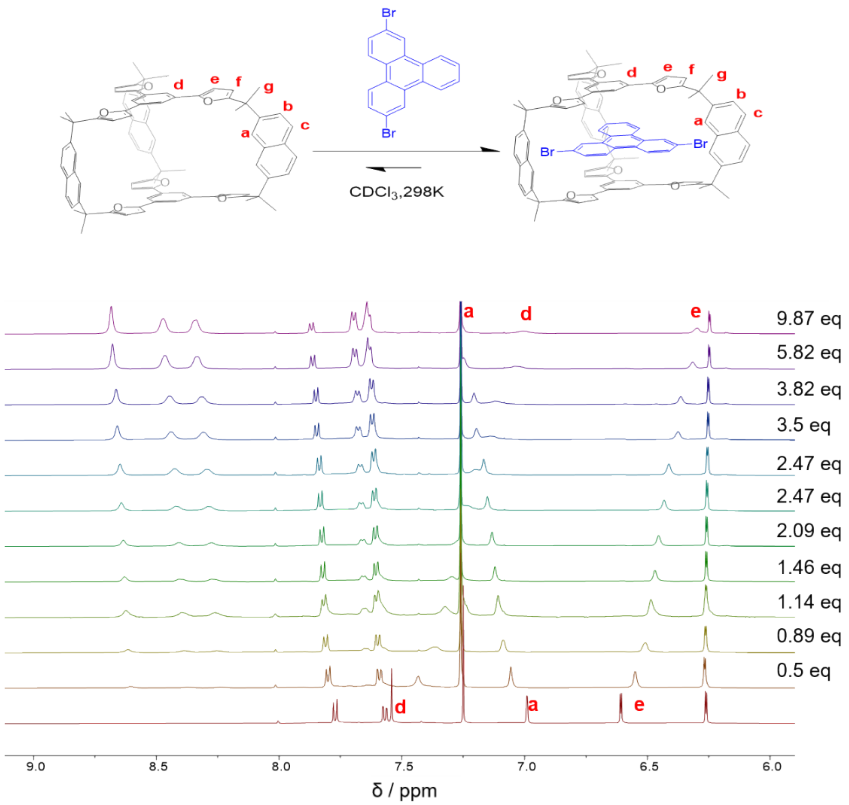

Figure S30. Partial ^{1}H NMR spectra (600 MHz, $CDCl_3$, 298 K) of **FPC** recorded after addition of different amount of **G11** from 0 equiv. (bottom) to 4.5 equiv. (top) with a constant concentration of **FPC** ([C] = 2.8 mM).

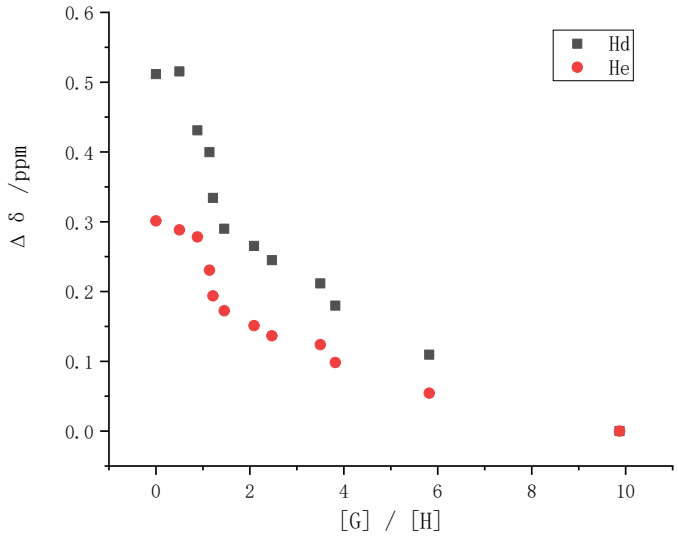

Figure S31. Plots of the chemical shift difference (Δδ)corresponding to the proton e (red) and proton d (black) versus the amount of the guest-to-host ratio. The data were fitted with 1:1 binding model and gave $K_a = (2.3 \pm 0.1) \times 10^3$ M^{-1}.

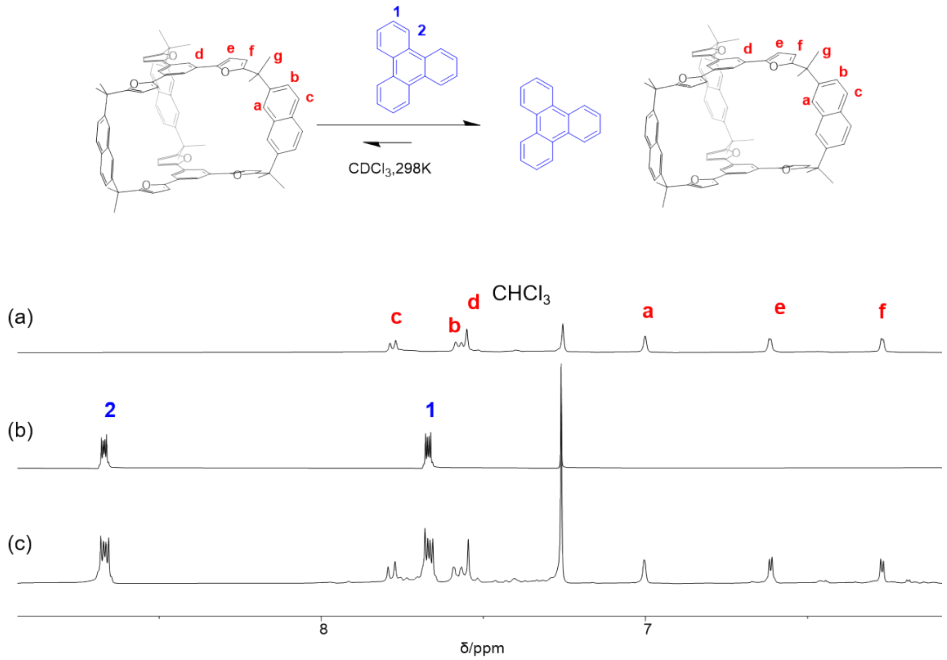

Figure S32. Partial ^{1}H NMR spectra (600 MHz, $CDCl_3$, 298 K) of (a) **FPC**. (b) Triphenylene. (c) **FPC** + Triphenylene (6 equiv.).

4. Photophysical Properties of the Charge Transfer Systems.

(a)

(b)

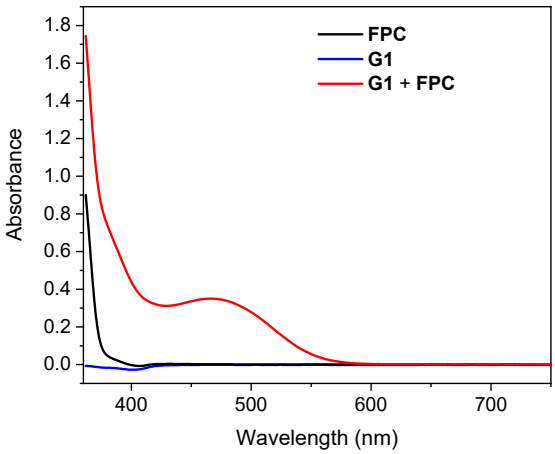

Figure S33. (a) The optical images show the solution color changes, from left to right: **FPC** ($CHCl_3$, 7.0mM), **G1** ($CHCl_3$, 7.0mM) and the mixture of **G1** and **FPC** under the same conditions. (b) UV-vis absorption spectrum of **G1** (black), **FPC** (red) and **G1⊂FPC** (blue) in $CHCl_3$ (2.5×10^{-5}M，298K).

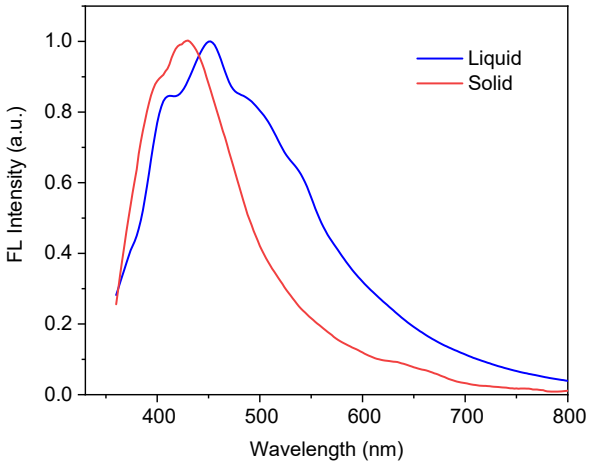

Figure S34. Normalized fluorescence emission spectra of **FPC** (λ_{ex} = 350 nm). Red line corresponding to the of the solid sample. Blue line corresponding to the solution sample in $CHCl_3$.

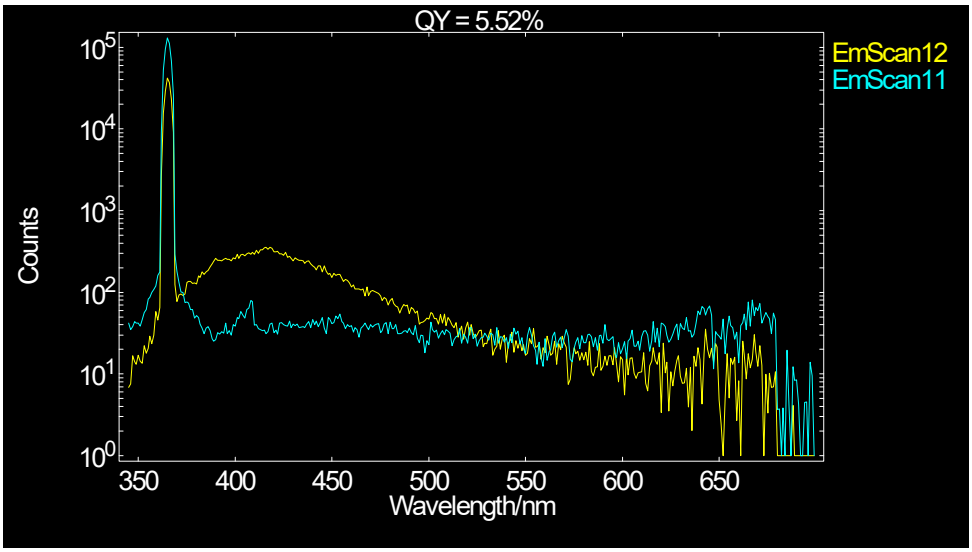

Figure S35. Fluorescence quantum efficiency of **FPC**.

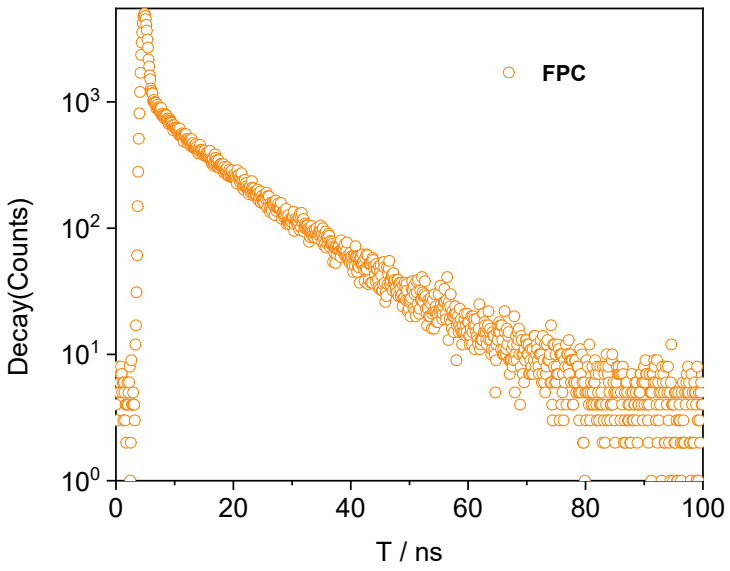

Figure S36. Fluorescence emission lifetime of **FPC** in the solid state (λ_{ex} = 360 nm, τ = 19.9 ns).

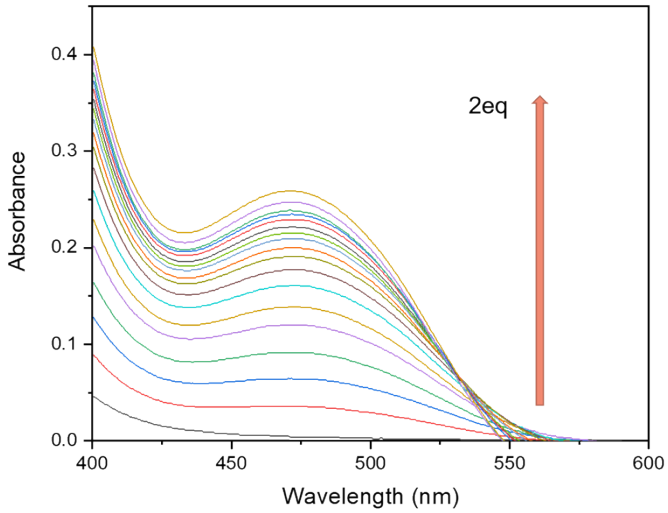

Figure S37. The alternation of UV-vis absorption in a chloroform solution (2.0 mM) after addition of different amount of **G1** in the **FPC** solution, from 0 (bottom) to 2 equiv. (top).

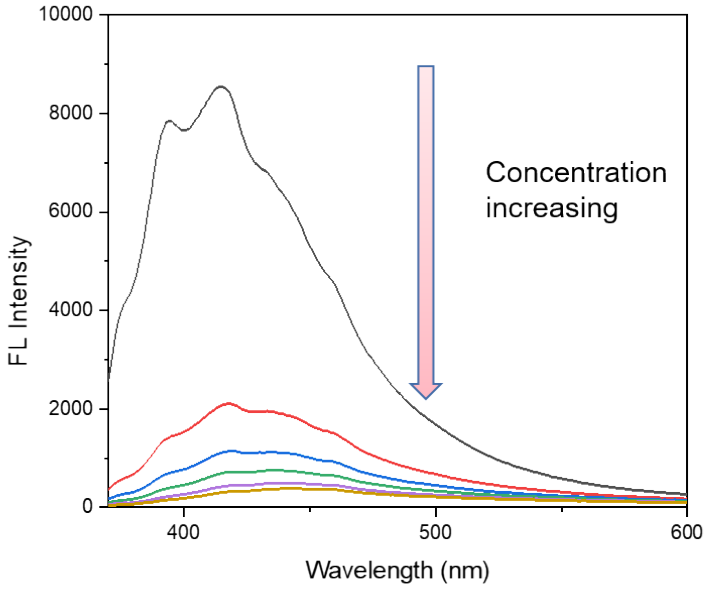

Figure S38. Fluorescence titration (λ_{ex} = 350 nm) of **FPC** (0.70 mM) in $CHCl_3$ at room temperature upon a gradual increase in the concentration of **G1** (from 0 to 0.35 mM).

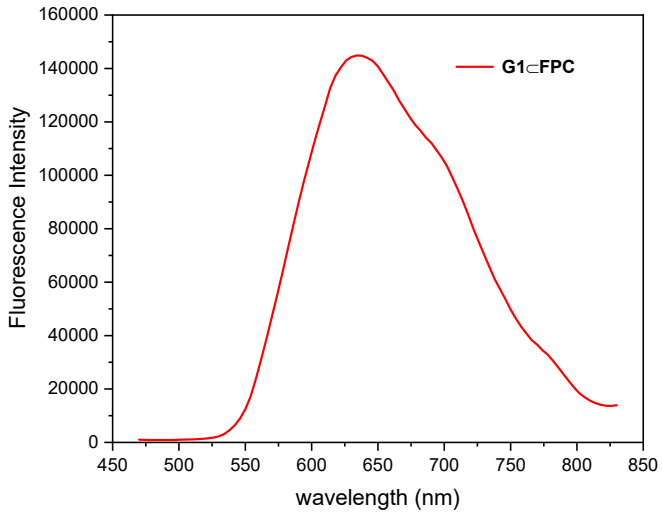

Figure S39. Normalized fluorescence emission spectra of cocrystal **G1⊂FPC** in the solid state (λ_{ex} = 460 nm).

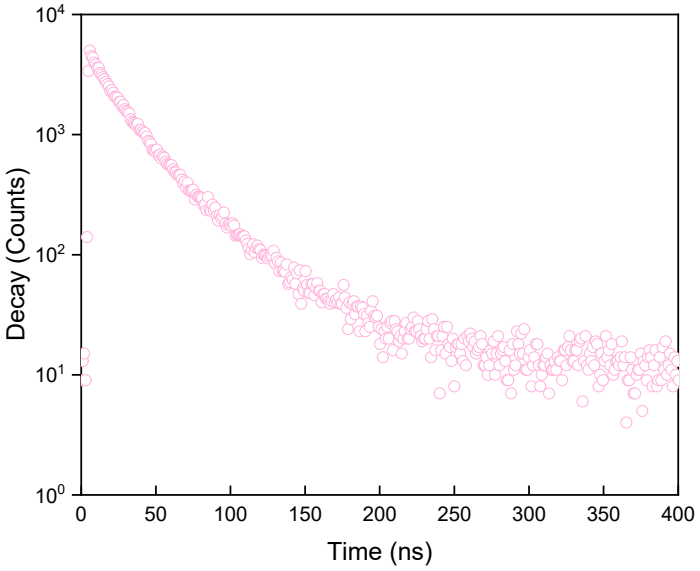

Figure S40. Fluorescence emission lifetime of **G1⊂FPC** in the solid state (λ_{ex} = 450 nm, τ = 33.5 ns).

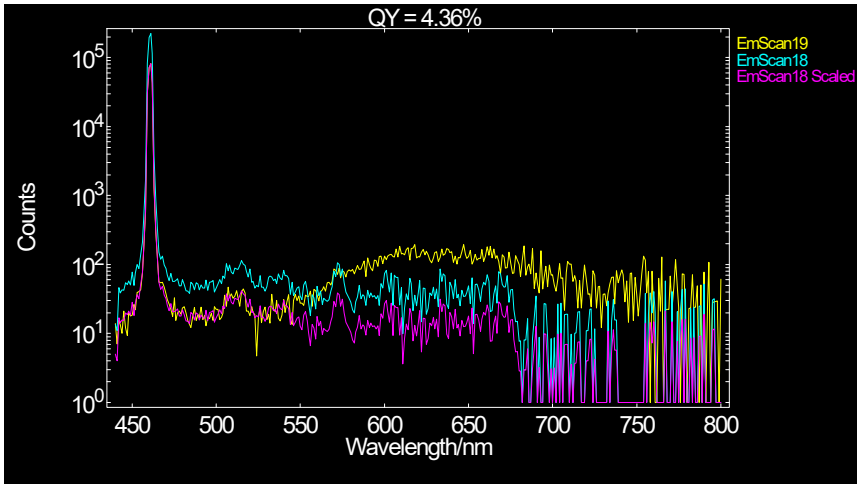

Figure S41. Fluorescence quantum efficiency of **G1⊂FPC**.

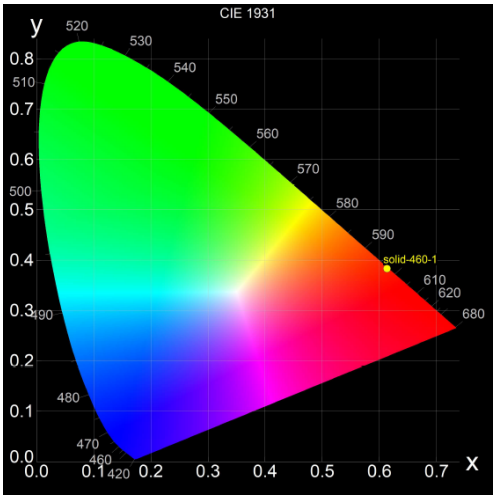

Figure S42. The CIE coordinate of **G1 ⊂ FPC**.

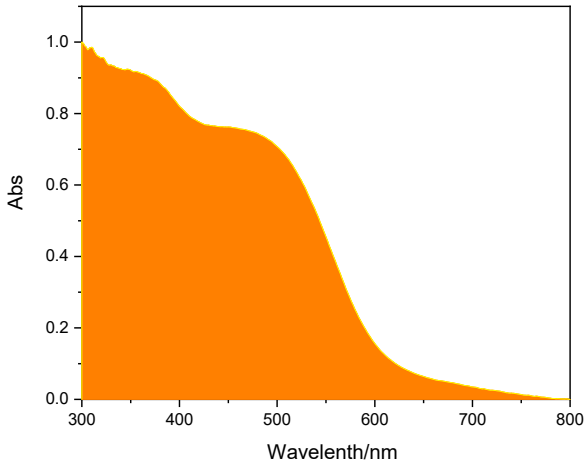

Figure S43. Normalized solid-state UV-vis absorption spectra of crystalline **G1⊂FPC**.

(a)

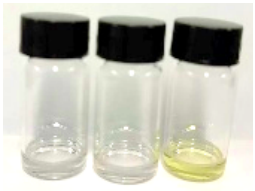

(b)

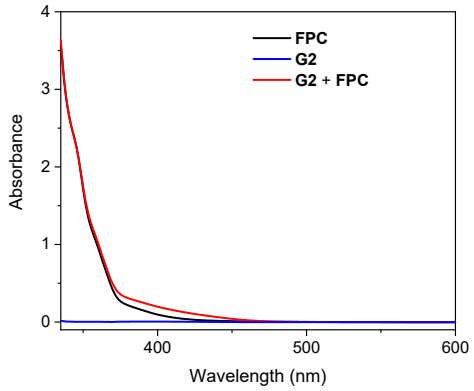

Figure S44. (a) The optical images show the solution color changes, from left to right: **FPC** ($CHCl_3$, 7.0 mM), **G2** ($CHCl_3$, 7.0 mM) and the mixture of **G2** and **FPC** under the same conditions. (b) UV-vis absorption spectrum of **FPC** (blue), **G2**(black) and **G2⊂FPC** (red) in $CHCl_3$ (7.0 mM，298 K).

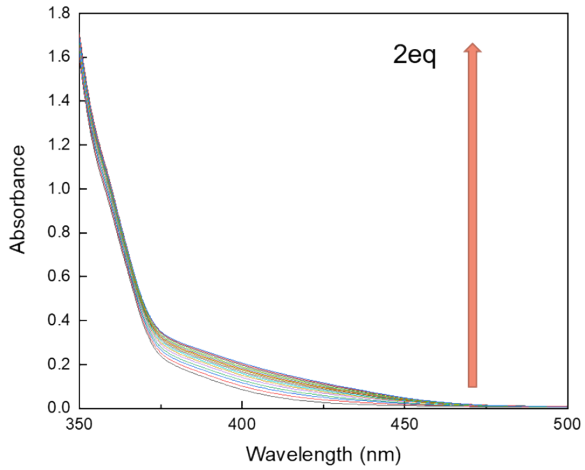

Figure S45. The alternation of UV-vis absorption in a chloroform solution (2.0 mM) after addition of different amount of **G2** in the **FPC** solution, from 0 (bottom) to 1.6 equiv. (top).

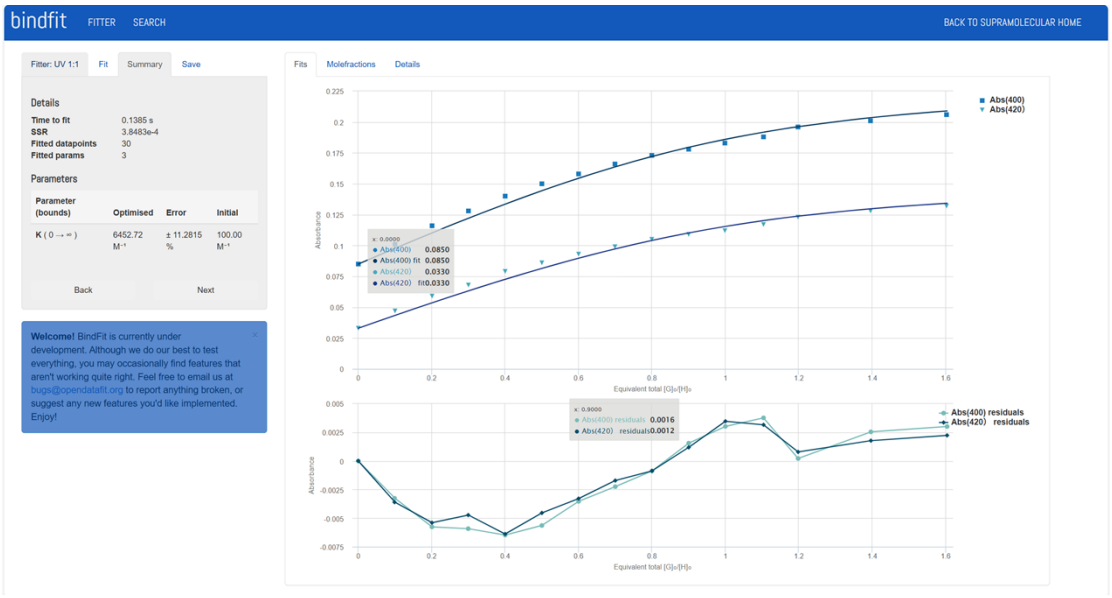

Figure S46. Plots of absorbance at 400 nm and 420 nm versus [**G2**]/ [**FPC**]. The data were fitted to a 1:1 binding model, giving K_a= (6.4±0.6) ×10^3 M^{-1}. All plots were obtained from non-linear curve-fitting to a 1:1 binding model using the www.supramolecular.org web applet.

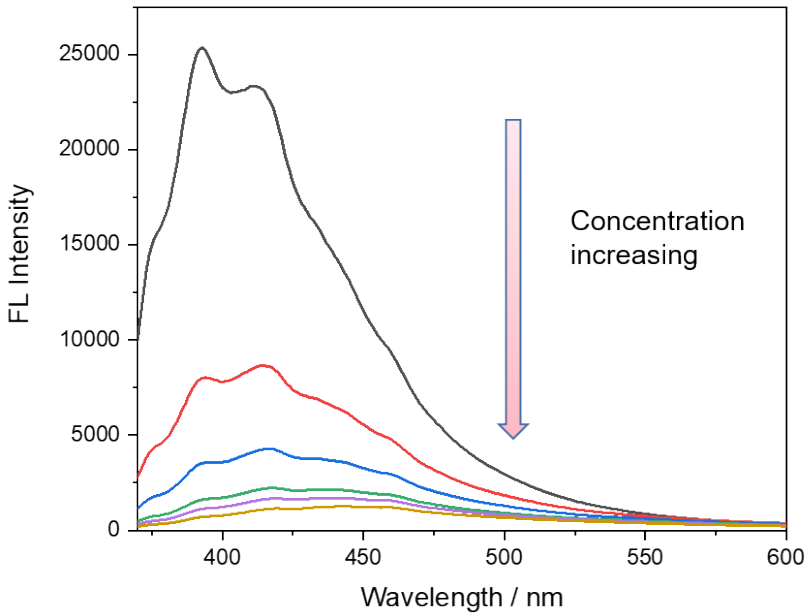

Figure S47. Fluorescence titration (λ_{ex} = 350 nm) of **FPC** (0.75 mM) in $CHCl_3$ at room temperature upon a gradual increase in the concentration of **G2** (from 0 to 0.38 mM).

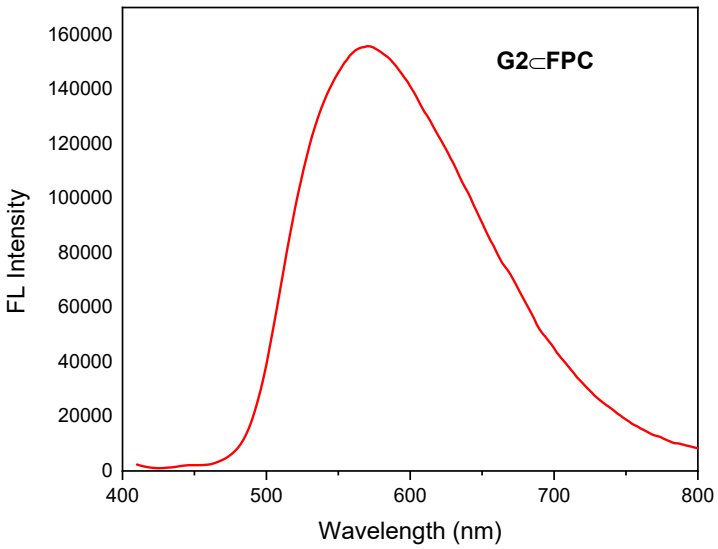

Figure S48. Normalized fluorescence emission spectra of cocrystal **G2⊂FPC** in the solid state (λ_{ex} = 400 nm).

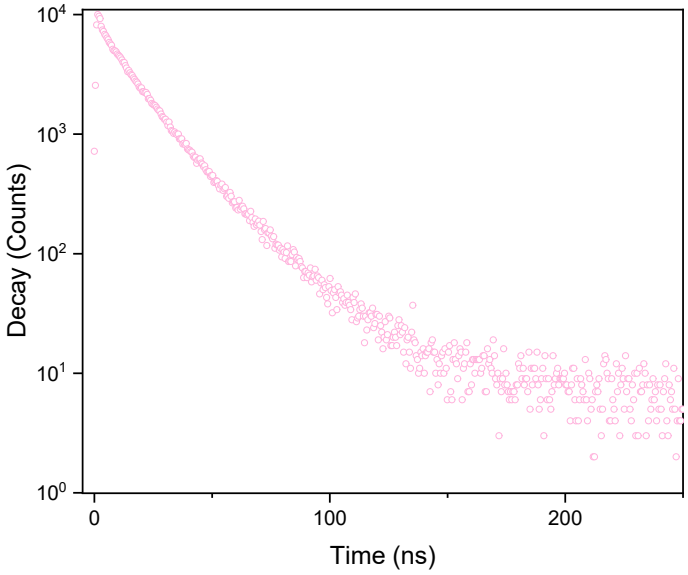

Figure S49. Fluorescence emission lifetime of **G2⊂FPC** in the solid state. (λ_{ex} = 360 nm, τ = 15.5 ns).

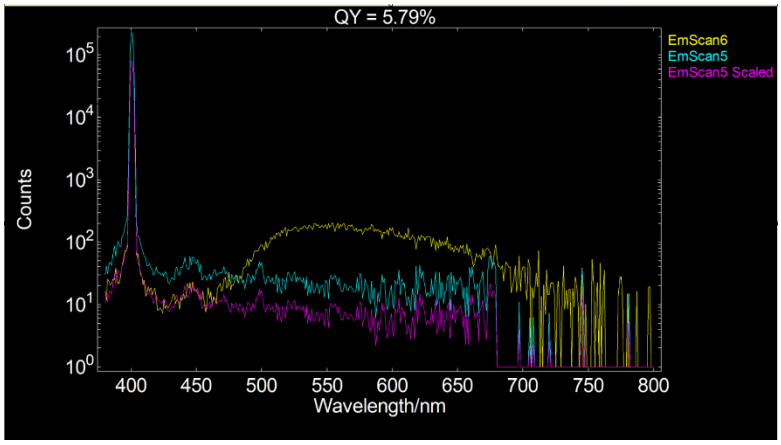

Figure S50. Fluorescence quantum efficiency of **G2⊂FPC**.

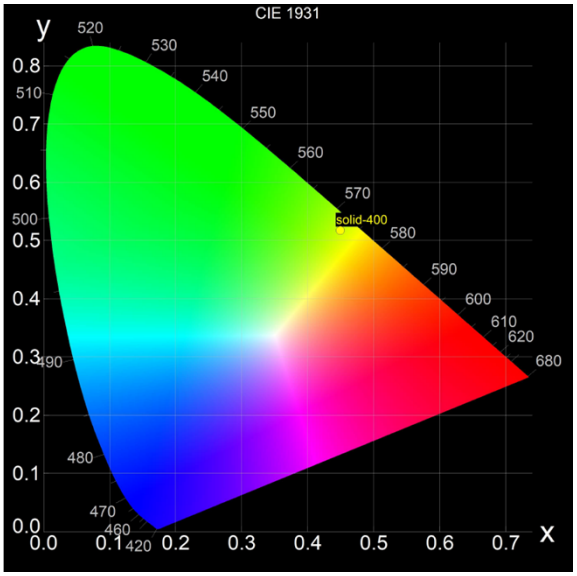

Figure S51. The CIE coordinates of **G2⊂FPC**.

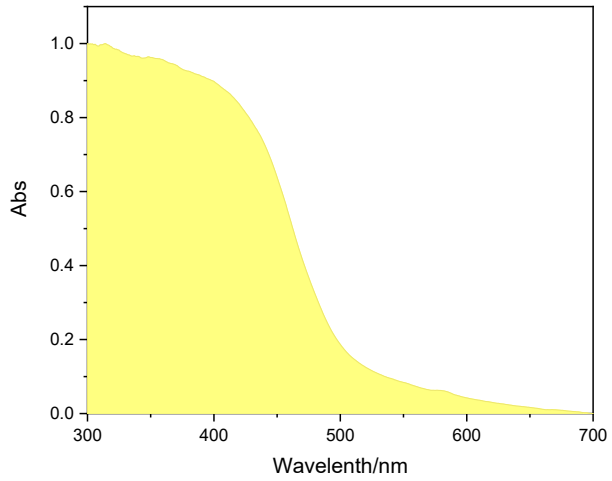

Figure S52. Normalized solid-state UV-vis absorption spectra of crystalline **G2⊂FPC**.

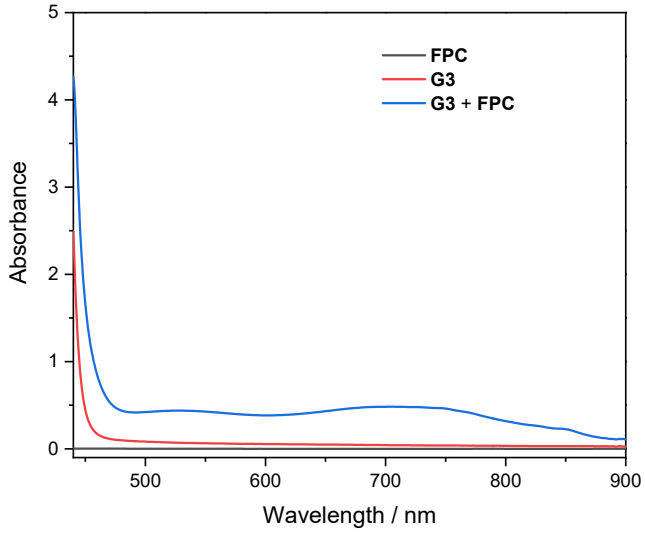

Figure S53. UV-vis absorption spectrum of **FPC** (black), **G3** (red) and **G3⊂FPC** (blue) in $CHCl_3$ (7.0 Mm, 298 K).

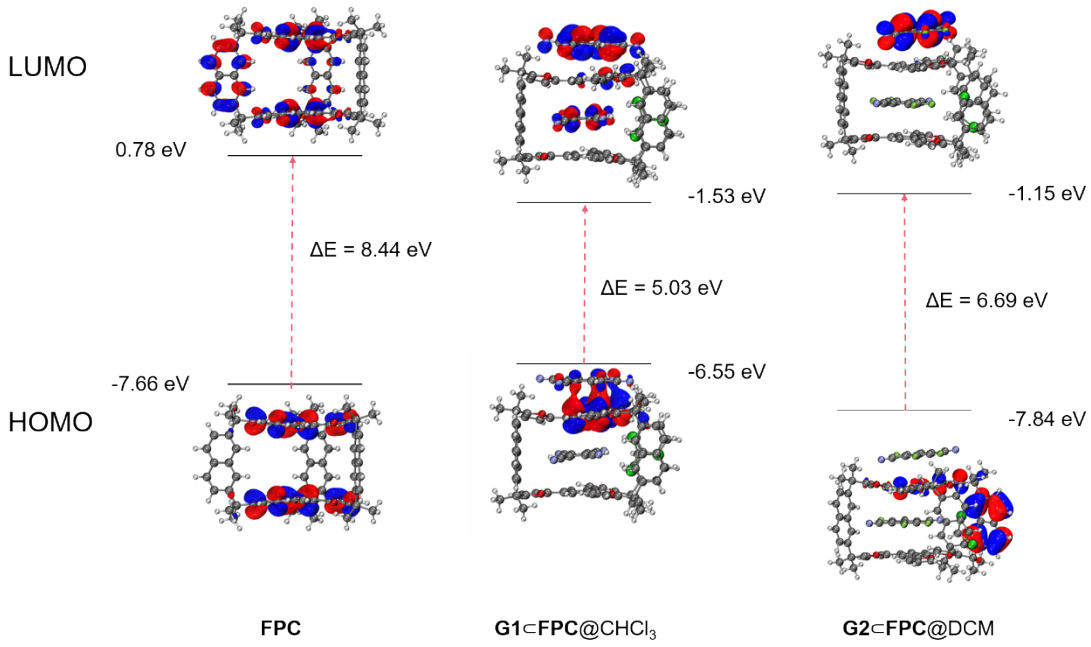

Figure S54. HOMO and LUMO distribution and frontier orbital energy levels calculation results of **FPC**, **G1⊂FPC**@$CHCl_3$ and **G2⊂FPC**@DCM.

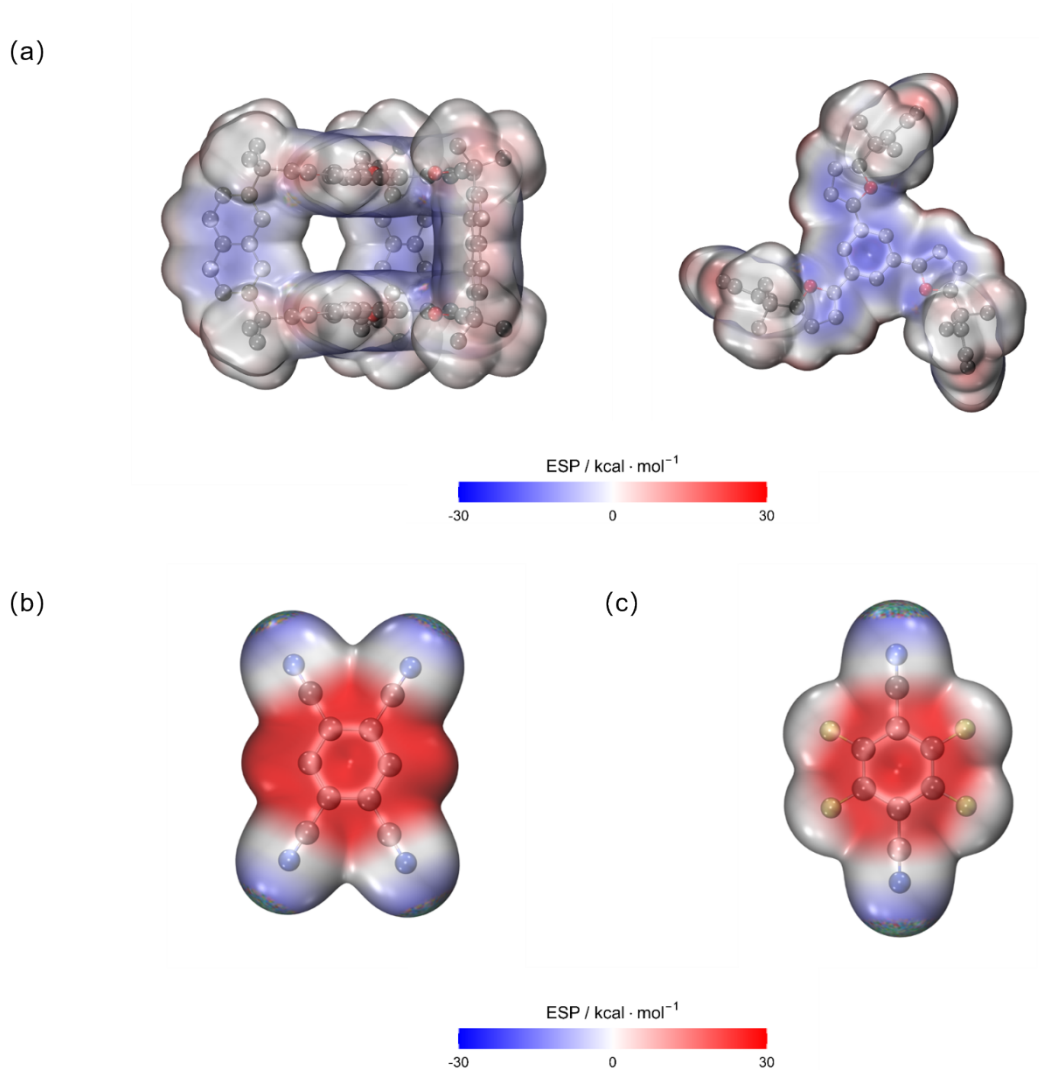

Figure S55. ESP maps of (a) **FPC** (top and side views). (b) **G1**. (c) **G2**.

5. Single crystal information.

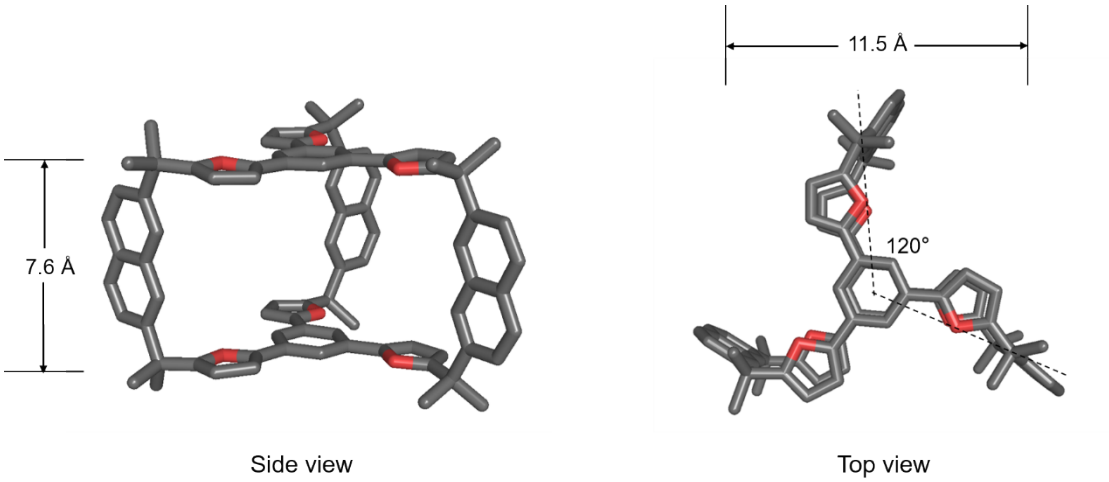

Figure S56.The single crystal structure of **FPC** showing a C_{3h} axis of symmetry. Left: the side view of the framework and right: the top view of the framework.

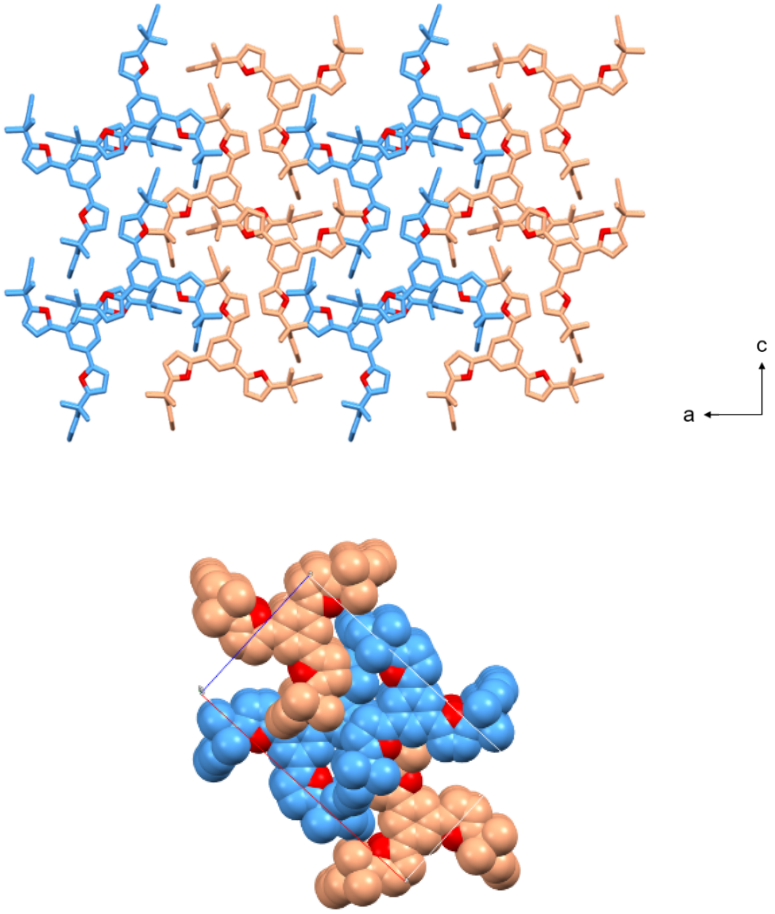

Figure S57. Layer-like packing structure formed by adjacent molecules in the *ac* plane. TOP: capped stick image. Bottom: spacefill image.

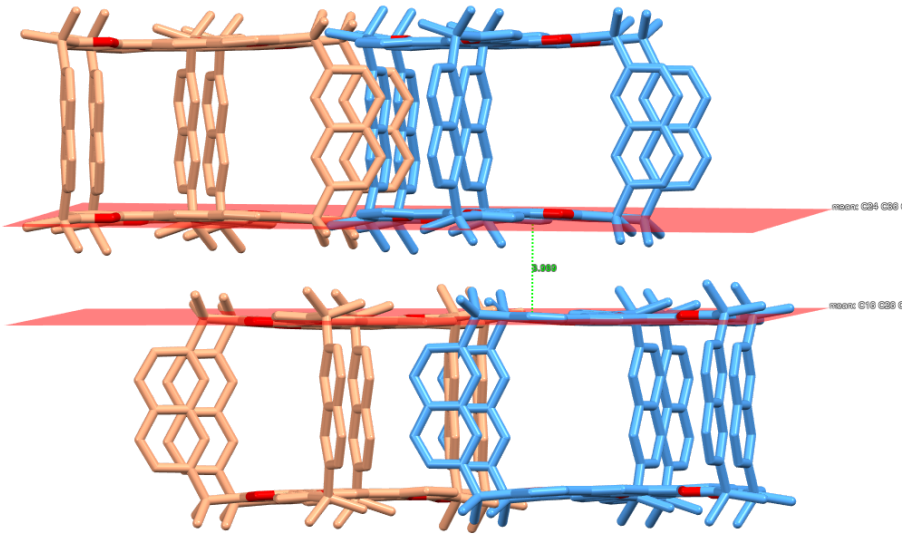

Figure S58. Side view of layer-like superstructure networks formed by **FPC**, π…π interactions between the adjacent TPB planes are labelled.

Table 1 Crystal data and structure refinement for Single-Crystal FPC

Empirical formula	$C_{168}H_{144}O_{12}$
Formula weight	2354.82
Temperature/K	223.00
Crystal system	orthorhombic
Space group	Pnma
a/Å	23.9792(9)
b/Å	23.1831(7)
c/Å	13.8712(5)
α /°	90
β /°	90
γ /°	90
Volume/Å^3	7711.2(5)
Z	2
ρ_{calc}g/cm^3	1.014
μ /mm^{-1}	0.063
F(000)	2496.0
Crystal size/mm^3	0.23 × 0.1 × 0.07
Radiation	MoKα (λ = 0.71073)
2θ range for data collection/°	3.82 to 50.076
Index ranges	-28 ⩽ h ⩽ 28, -27 ⩽ k ⩽ 27, -16 ⩽ l ⩽ 16
Reflections collected	122007
Independent reflections	7005 [R_{int} = 0.0954, R_{sigma} = 0.0284]
Data/restraints/parameters	7005/0/421
Goodness-of-fit on F^2	1.051
Final R indexes [I>=2σ (I)]	R_1 = 0.0482, wR_2 = 0.1352
Final R indexes [all data]	R_1 = 0.0676, wR_2 = 0.1495
Largest diff. peak/hole / e Å^{-3}	0.40/-0.26
CCDC number	2422476

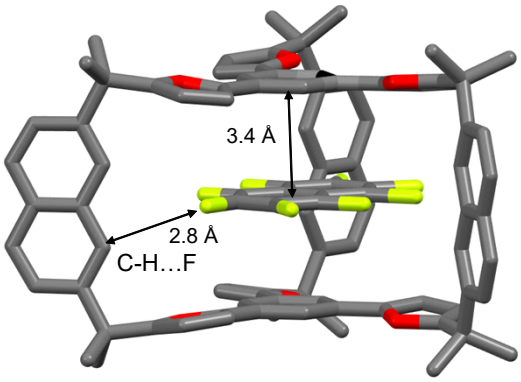

Figure S59. The single crystal structure of the complex **G4⊂FPC**. The existence of π…π interactions between guests and TPB planes and C-H···F hydrogen bonds are labelled.

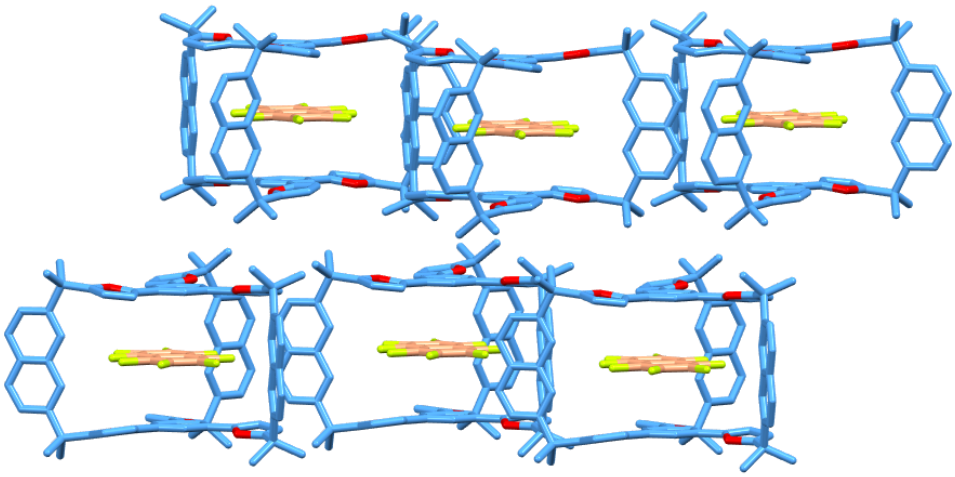

Figure S60. Illustration of layer-like superstructure formed by **G4⊂FPC**.

Table 2. Crystal data and structure refinement for Single-Crystal（G4⊂FPC）

Empirical formula	$C_{94}H_{72}F_8O_6$
Formula weight	1449.51
Temperature/K	170.00
Crystal system	hexagonal
Space group	$P6_3/m$
a/Å	14.1009(3)
b/Å	14.1009(3)
c/Å	22.9661(10)
α/°	90
β/°	90
γ/°	120
Volume/Å^3	3954.7(2)
Z	2
ρ_{calc}g/cm^3	1.217
μ/mm^{-1}	0.461
F(000)	1512.0
Crystal size/mm^3	0.23 × 0.1 × 0.07
Radiation	GaKα (λ = 1.34139)
2θ range for data collection/°	6.296 to 121.234
Index ranges	$-17 \le h \le 17$, $-18 \le k \le 18$, $-29 \le l \le 29$
Reflections collected	21014
Independent reflections	3100 [R_{int} = 0.0621, R_{sigma} = 0.0822]
Data/restraints/parameters	3100/241/261
Goodness-of-fit on F^2	1.049
Final R indexes [I>=2σ (I)]	R_1 = 0.0651, wR_2 = 0.1816
Final R indexes [all data]	R_1 = 0.0770, wR_2 = 0.1917
Largest diff. peak/hole / e Å^{-3}	0.40/-0.38
CCDC number	2430685

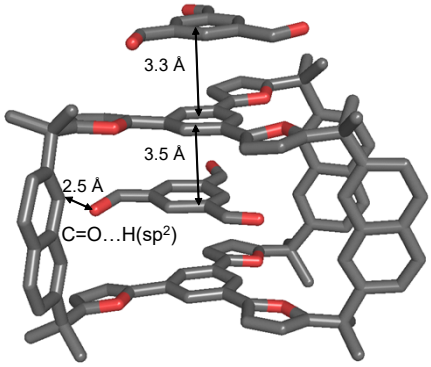

Figure S61. The single crystal structure of the complex **G5⊂FPC.** The existence of π…π interactions between guests and TPB planes and hydrogen bonds between guests and aromatic hydrogens are labelled. The framework exhibits a little distortion compared to compound **FPC** due to the presence of the hydrogen bonds.

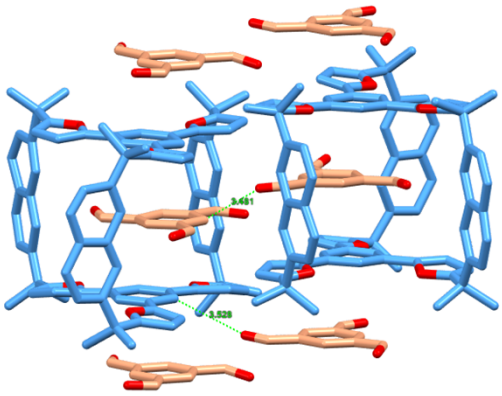

Figure S62. Illustration of various C-H···O hydrogen bonds between adjacent units in the crystal structure of the complex **G5⊂FPC**.

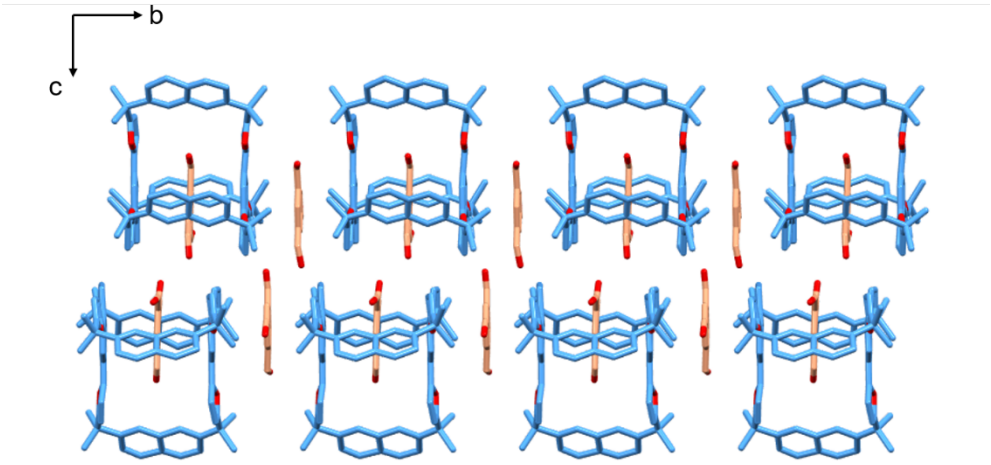

Figure S63. Illustration of the "sandwich"-like superstructure in the *bc* plane, revealing an array arrangement based on π…π interactions with a 1:2 host-guest ratio in the crystal structure of the complex **G5 ⊂FPC**.

Table 3. Crystal data and structure refinement for Single-Crystal（G5⊂FPC）

Empirical formula	$C_{104}H_{86}Cl_6O_{12}$
Formula weight	1740.42
Temperature/K	170.00
Crystal system	monoclinic
Space group	Cc
a/Å	36.710(2)
b/Å	13.5712(9)
c/Å	42.156(3)
α/°	90
β/°	113.644(3)
γ/°	90
Volume/Å^3	19239(2)
Z	8
ρ_{calc}g/cm^3	1.202
μ/mm^{-1}	1.384
F(000)	7264.0
Crystal size/mm^3	0.17 × 0.17 × 0.05
Radiation	GaKα (λ = 1.34139)
2θ range for data collection/°	6.11 to 110.358
Index ranges	-44 ≤ h ≤ 42, -15 ≤ k ≤ 16, -51 ≤ l ≤ 51
Reflections collected	108224
Independent reflections	34483 [R_{int} = 0.0654, R_{sigma} = 0.0671]
Data/restraints/parameters	34483/244/2199
Goodness-of-fit on F^2	1.274
Final R indexes [I>=2σ (I)]	R_1 = 0.1282, wR_2 = 0.2948
Final R indexes [all data]	R_1 = 0.1455, wR_2 = 0.3041
Largest diff. peak/hole / e Å^{-3}	0.66/-0.70
Flack parameter	0.52(5)
CCDC number	2422477

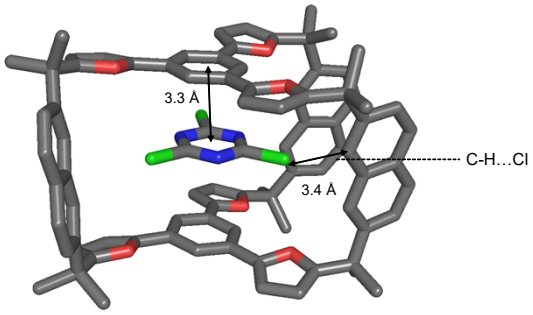

Figure S64. The single crystal structure of the complex **G6⊂FPC**. The existence of π…π interactions between guests and TPB planes and hydrogen bonds between guests and aromatic hydrogens are labelled. The framework exhibits a little distortion compared to compound **FPC** due to the presence of the hydrogen bonds.

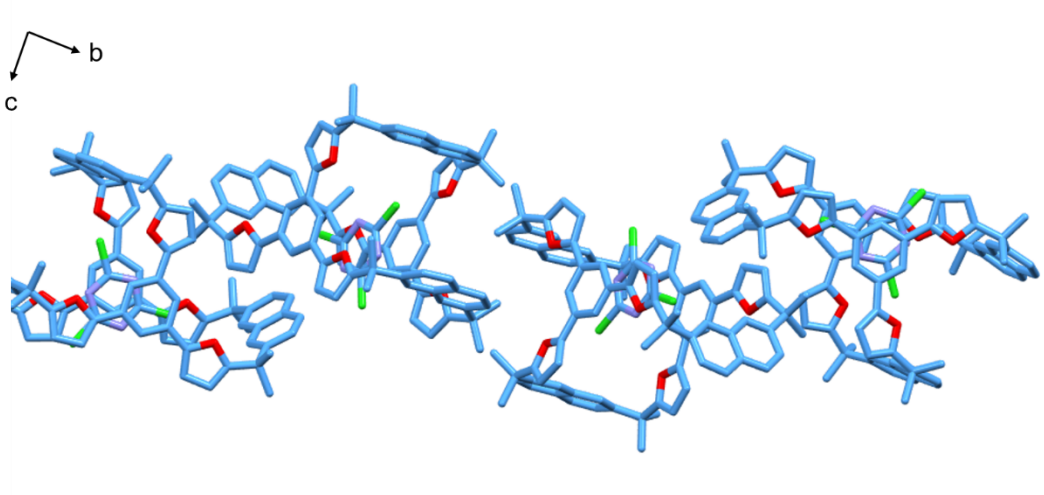

Figure S65. Illustration of packing mode of **G6⊂FPC**.

Table 4. Crystal data and structure refinement for Single-Crystal（G6⊂FPC）

Empirical formula	$C_{87}H_{72}Cl_3N_3O_6$
Formula weight	1361.82
Temperature/K	170.00
Crystal system	monoclinic
Space group	$P2_1/c$
a/Å	13.0442(3)
b/Å	45.4447(11)
c/Å	12.4711(3)
α/°	90
β/°	105.2980(10)
γ/°	90
Volume/Å^3	7130.8(3)
Z	4
ρ_{calc}g/cm^3	1.269
μ/mm^{-1}	1.065
F(000)	2856.0
Crystal size/mm^3	0.17 × 0.17 × 0.05
Radiation	GaKα (λ = 1.34139)
2θ range for data collection/°	6.112 to 109.908
Index ranges	-15 ≤ h ≤ 15, -55 ≤ k ≤ 55, -15 ≤ l ≤ 14
Reflections collected	166835
Independent reflections	13544 [R_{int} = 0.0835, R_{sigma} = 0.0365]
Data/restraints/parameters	13544/0/904
Goodness-of-fit on F^2	1.034
Final R indexes [I>=2σ (I)]	R_1 = 0.0557, wR_2 = 0.1375
Final R indexes [all data]	R_1 = 0.0820, wR_2 = 0.1548
Largest diff. peak/hole / e Å^{-3}	0.41/-0.66
CCDC number	2422478

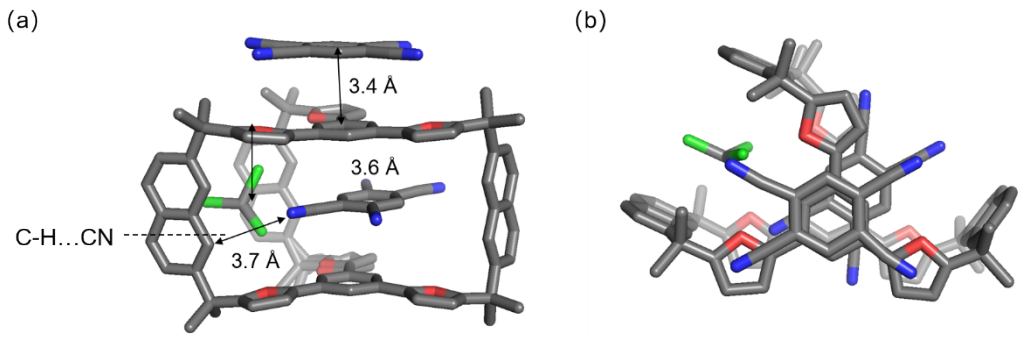

Figure S66. (a) Side view of the single crystal structure of the complex **G1⊂FPC**. The existence of π…π interactions between guests and TPB planes and hydrogen bonds between guests and aromatic hydrogens are labelled. (b) Top view of the complex, which shows slightly distortion due to the hydrogen bonds.

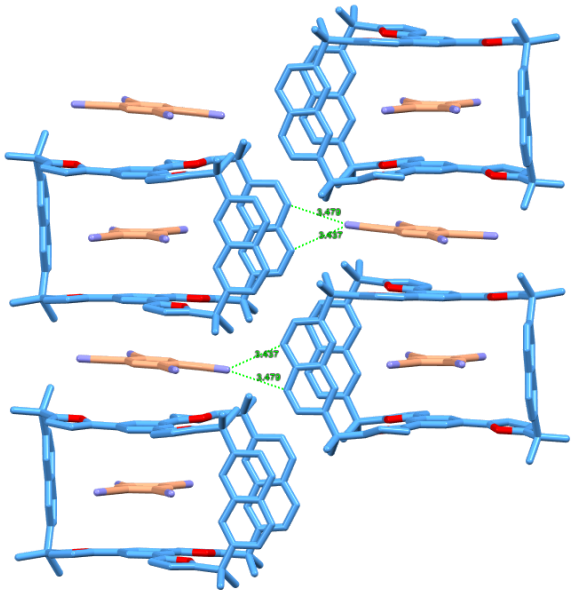

Figure S67. Illustration of various C-H···N hydrogen bonds between adjacent units in the crystal structure of the complex **G1⊂FPC**.

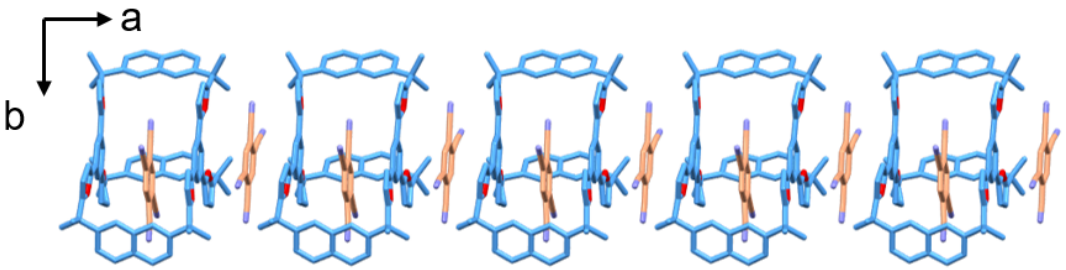

Figure S68. Illustration of the "sandwich"- like superstructure in the *ab* plane, revealing an arrayed arrangement arising from π…π interactions with a 1:2 host–guest ratio in the crystal structure of the complex **G1⊂FPC**. For clarity, hydrogen atoms and $CHCl_3$ molecules have been omitted.

Table 5. Crystal data and structure refinement for Single-Crystal（G1⊂FPC）

Empirical formula	$C_{108}H_{82}Cl_{12}N_8O_6$
Formula weight	2013.21
Temperature/K	170.00
Crystal system	triclinic
Space group	P-1
a/Å	13.530(3)
b/Å	17.329(3)
c/Å	22.136(4)
α/°	106.899(5)
β/°	98.618(4)
γ/°	91.523(6)
Volume/Å^3	4896.2(16)
Z	2
ρ_{calc}g/cm^3	1.366
μ/mm^{-1}	2.421
F(000)	2076.0
Crystal size/mm^3	0.1 × 0.06 × 0.03
Radiation	GaKα (λ = 1.34139)
2θ range for data collection/°	6.308 to 98.298
Index ranges	-15 ≤ h ≤ 14, -19 ≤ k ≤ 19, -24 ≤ l ≤ 20
Reflections collected	32644
Independent reflections	14408 [R_{int} = 0.0879, R_{sigma} = 0.1486]
Data/restraints/parameters	14408/454/1174
Goodness-of-fit on F^2	1.034
Final R indexes [I>=2σ (I)]	R_1 = 0.1197, wR_2 = 0.3164
Final R indexes [all data]	R_1 = 0.2332, wR_2 = 0.3950
Largest diff. peak/hole / e Å^{-3}	1.15/-0.49
CCDC	2497980

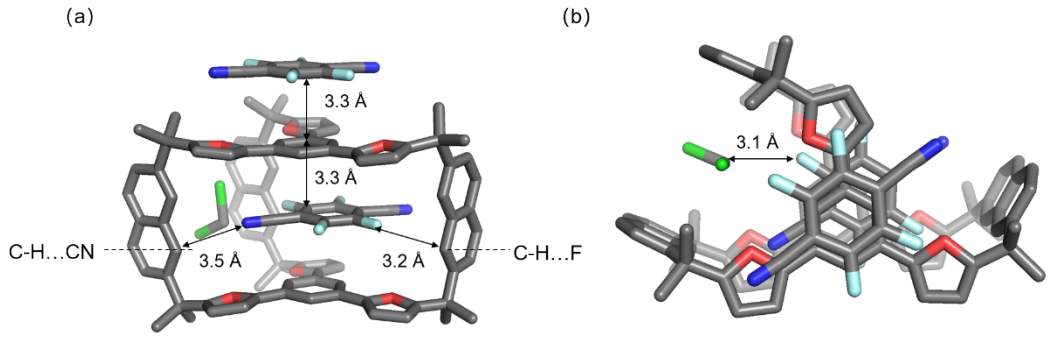

Figure S69. (a) Side view of the single crystal structure of the complex **G2⊂FPC**. The existence of π…π interactions between guests and TPB planes and hydrogen bonds between guests and aromatic hydrogens are labelled. (b) Top view of the complex, which shows distortion due to the hydrogen bonds.

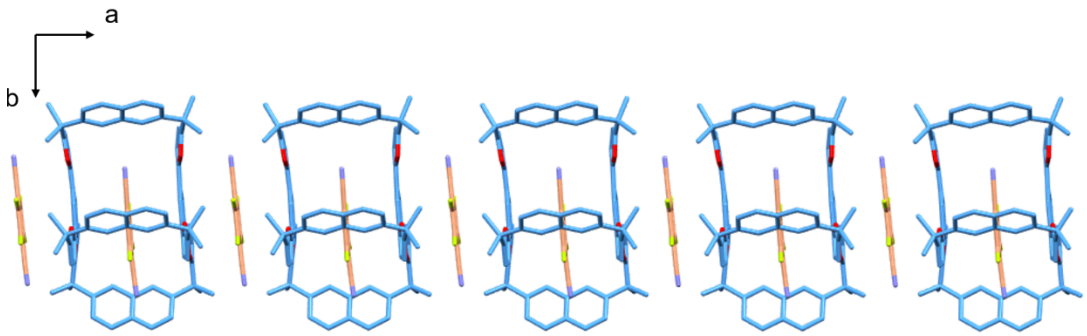

Figure S70. Illustration of the "sandwich"-like superstructure in the *ab* plane, revealing an arrayed arrangement arising from π…π interactions with a 1:2 host–guest ratio in the crystal structure of the complex **G2⊂FPC**. For clarity, hydrogen atoms and DCM molecules have been omitted.

Table 6. Crystal data and structure refinement for Single-Crystal（G2⊂FPC）

Empirical formula	$C_{101}H_{73}Cl_2F_8N_4O_6$
Formula weight	1661.53
Temperature/K	170.00
Crystal system	triclinic
Space group	P-1
a/Å	13.4122(13)
b/Å	17.5105(17)
c/Å	21.7230(17)
α/°	71.301(3)
β/°	82.345(4)
γ/°	85.423(4)
Volume/Å^3	4785.6(8)
Z	2
ρ_{calc}g/cm^3	1.153
μ/mm^{-1}	0.784
F(000)	1722.0
Crystal size/mm^3	0.26 × 0.03 × 0.03
Radiation	GaKα (λ = 1.34139)
2θ range for data collection/°	5.788 to 105
Index ranges	-14 ≤ h ≤ 15, -20 ≤ k ≤ 20, -25 ≤ l ≤ 25
Reflections collected	50363
Independent reflections	16253 [R_{int} = 0.0888, R_{sigma} = 0.1322]
Data/restraints/parameters	16253/1/1102
Goodness-of-fit on F^2	0.984
Final R indexes [I>=2σ (I)]	R_1 = 0.0876, wR_2 = 0.2399
Final R indexes [all data]	R_1 = 0.1610, wR_2 = 0.2957
Largest diff. peak/hole / e Å^{-3}	0.47/-0.53
CCDC	2501604

6. Job-Plot Analysis of Typical Host-Guest complexes.

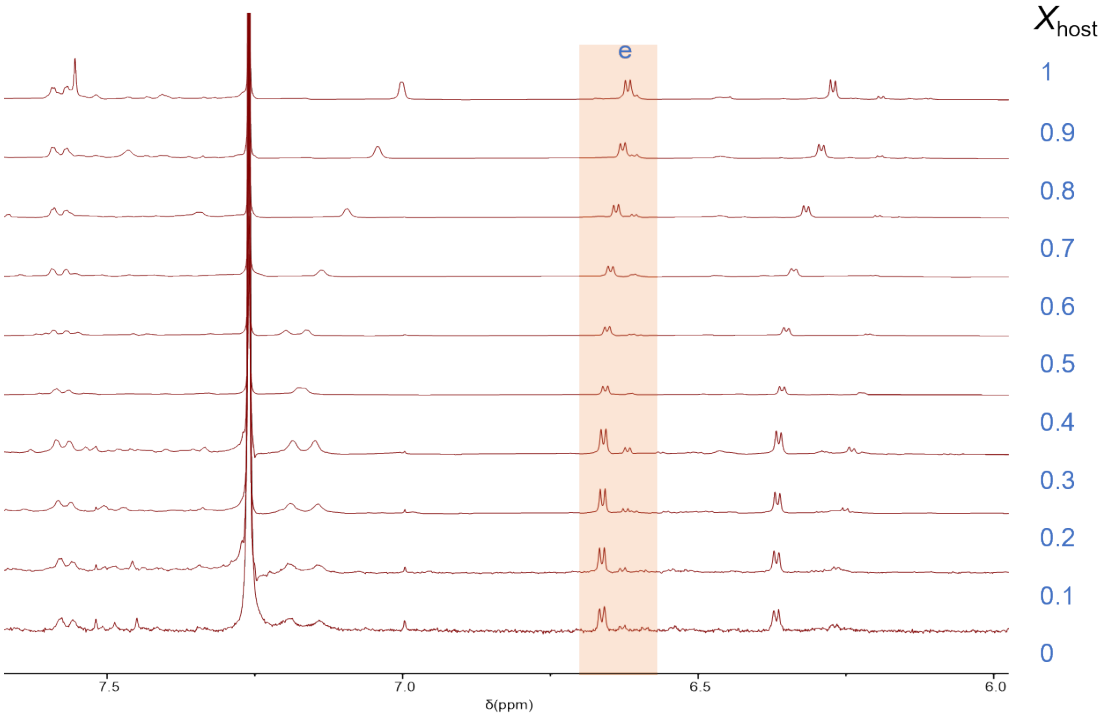

Figure S71. ^{1}H NMR spectra (400 MHz, $CDCl_3$, 298 K) of **FPC** in the presence of different amounts of **G1**. [**G1**] + [**FPC**] = 2.8 mM for all spectra. The Δδ of the proton H_e was used to make the Job plot.

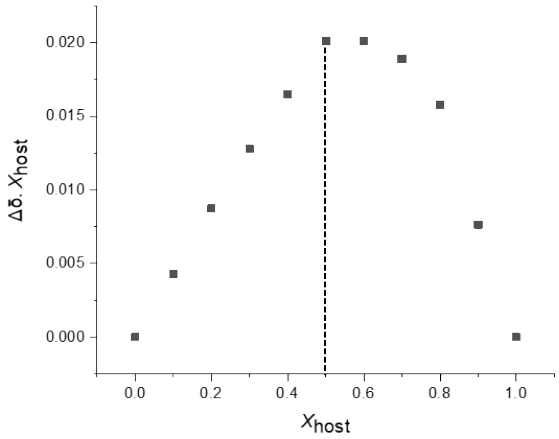

Figure S72. A Job plot of $\Delta\delta \cdot X_{host}$ versus X_{host}, based on the results in Figure S71.

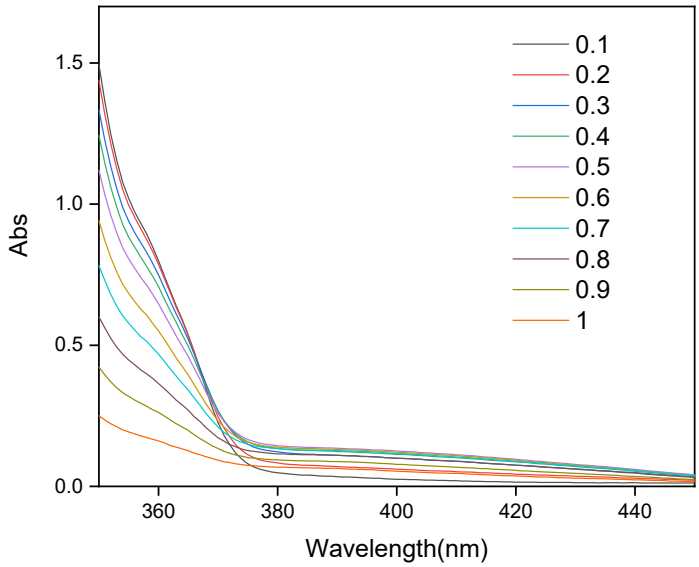

Figure S73. UV–vis spectra of **FPC** in the presence of varying amounts of **G2** were recorded while maintaining a constant total concentration ([**G2**] + [FPC] = 1.0 mM). The mole fraction of **FPC** was varied from 0 to 1. The changes in absorbance (ΔA) at the characteristic charge-transfer band were used to construct the Job plot.

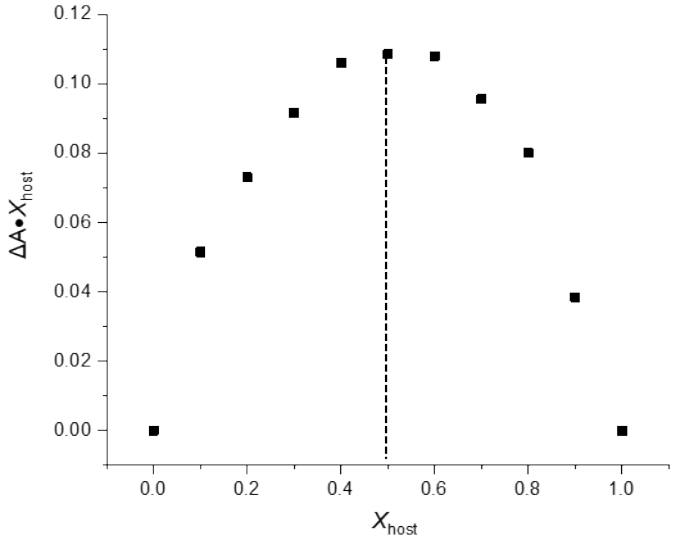

Figure S74. A Job plot of $\Delta A \cdot X_{host}$ versus X_{host}, based on the results in Figure S73.

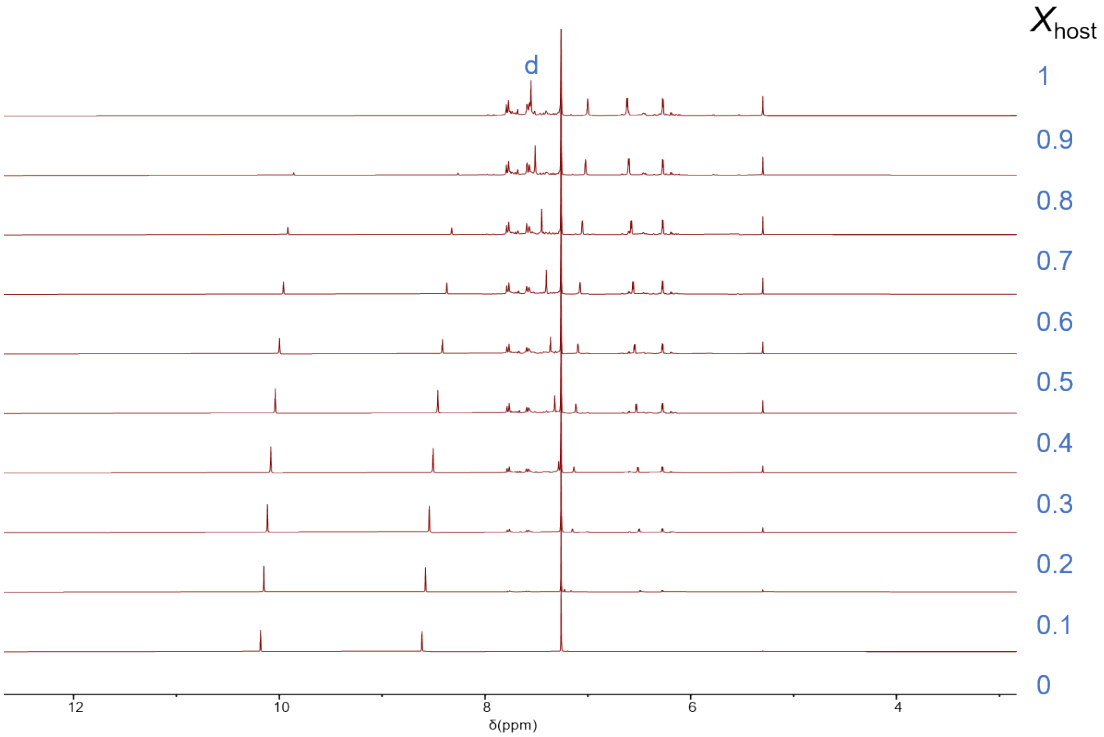

Figure S75. ^{1}H NMR spectra (400 MHz, $CDCl_3$, 298 K) of **FPC** in the presence of different amounts of **G5**. [**G5**] + [**FPC**] = 3 mM for all spectra. The Δδ of the proton H_d was used to make the Job plot.

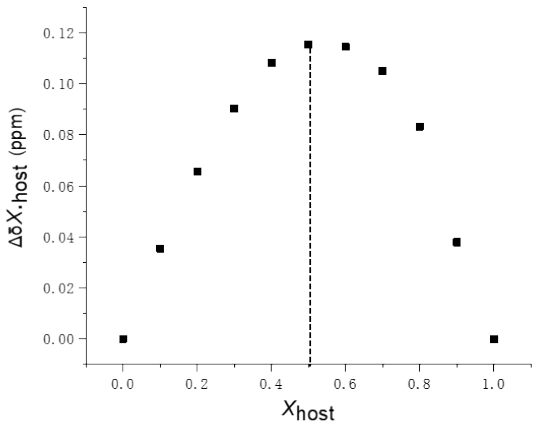

Figure S76. A Job plot of $\Delta\delta \cdot X_{host}$ versus X_{host}, based on the results in Figure S75.

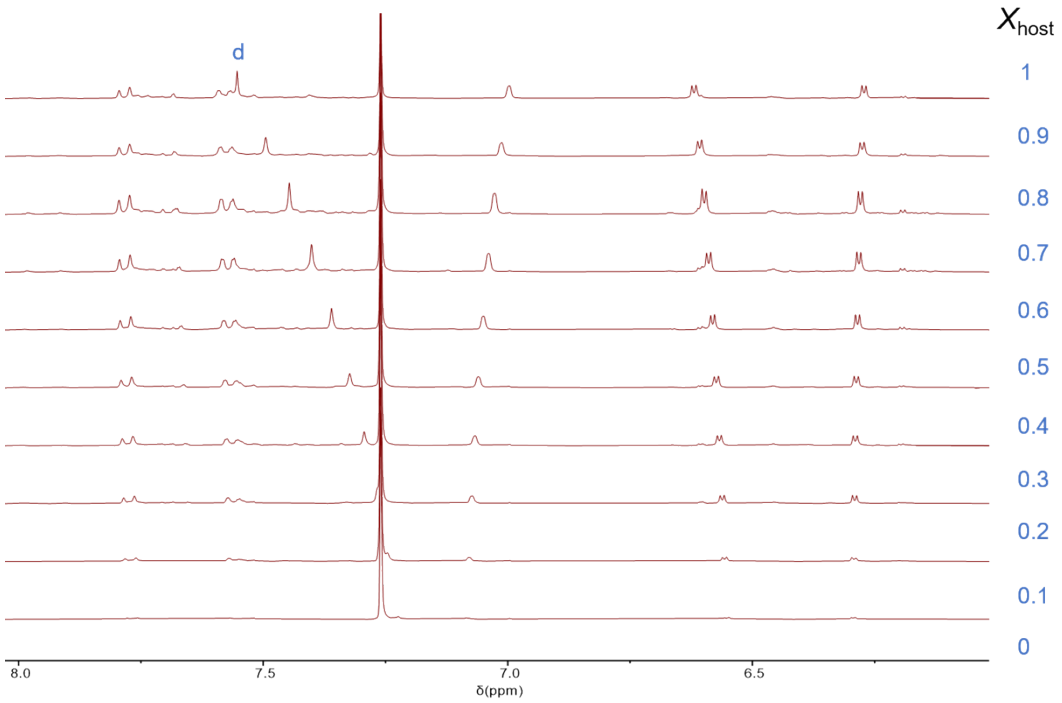

Figure S77. ^{1}H NMR spectra (400 MHz, $CDCl_3$, 298 K) of **FPC** in the presence of different amounts of **G4**. [**G4**] + [**FPC**] = 3 mM for all spectra. The Δδ of the proton H_d was used to make the Job plot.

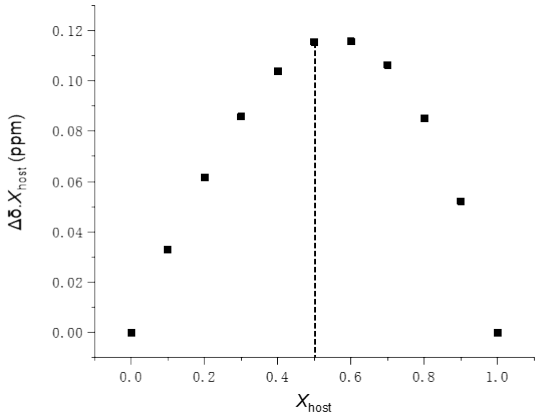

Figure S78. A Job plot of $\Delta\delta \cdot X_{host}$ versus X_{host}, based on the results in Figure S77.

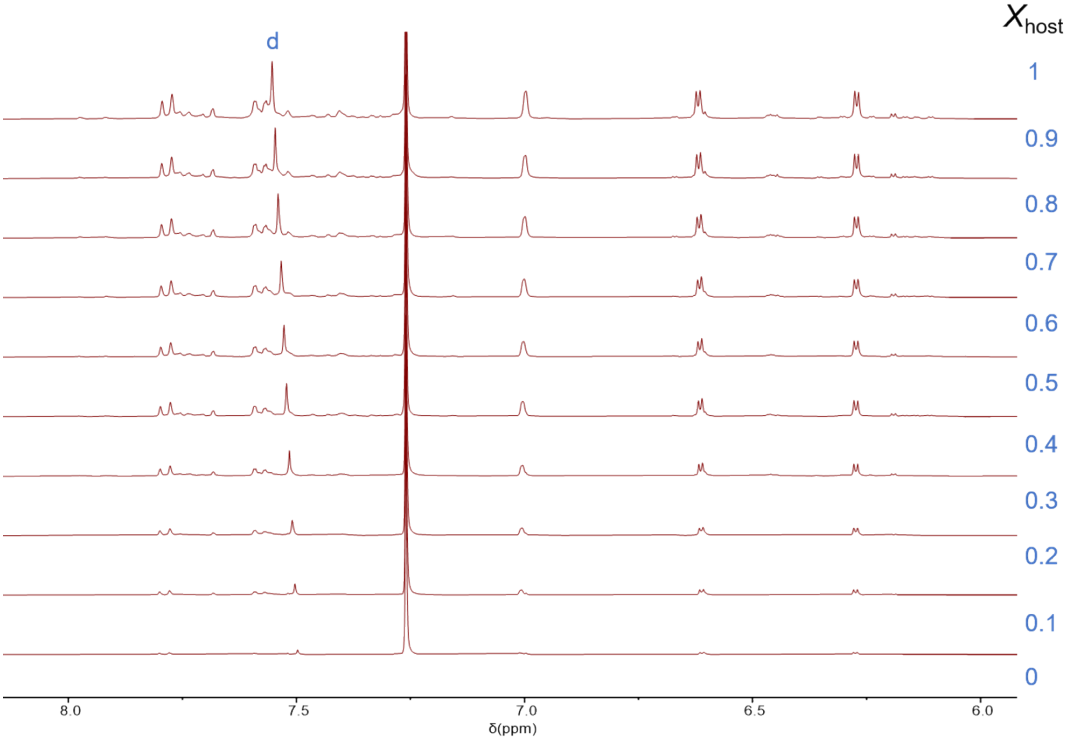

Figure S79. ^{1}H NMR spectra (400 MHz, $CDCl_3$, 298 K) of **FPC** in the presence of different amounts of **G6**. [**G6**] + [**FPC**] = 3 mM for all spectra. The Δδ of the proton H_d was used to make the Job plot.

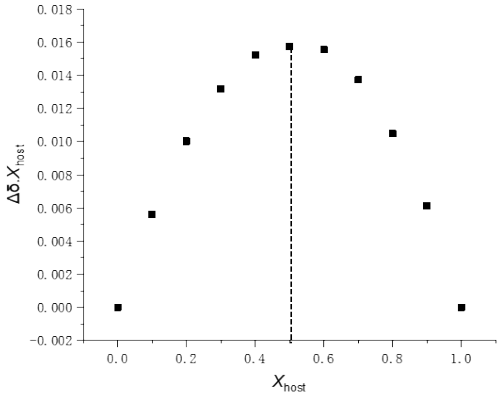

Figure S80. A Job plot of $\Delta\delta \cdot X_{host}$ versus X_{host}, based on the results in Figure S77.

7. Vapochromic behaviors of complex G1⊂ FPC.

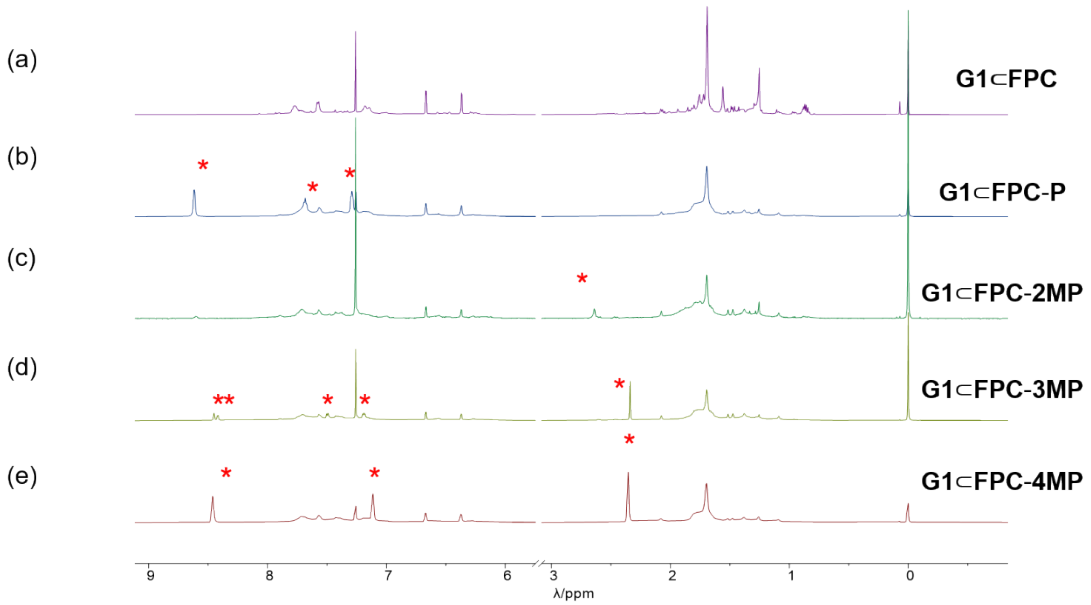

Figure S81. Partial ^{1}H NMR (298 K, 600 MHz, $CDCl_3$) of (a) **G1⊂ FPC** (b) **G1⊂FPC-P** (c) **G1⊂FPC-2MP** (d) **G1⊂FPC-3MP** and (e) **G1⊂FPC-4MP**.

8. Reference.

[S1] Zhu, D.; Sun, B.; Tong, L.; Wu, Y.; Cetin, M. M.; Li, H. A π-Electron Rich Cage via the Friedel-Crafts Reaction. *Org Lett*, **24**, 8980-8985 (2022).

[S2] Computational details

All the DFT calculations were performed with ORCA program [https://doi.org/10.1002/wcms.81 https://doi.org/10.1002/wcms.70019]. For geometry optimization and frequency analysis we adopted the hybrid functional by using the B3LYP [https://doi.org/10.1063/1.464913 https://doi.org/10.1103/PhysRevB.37.785] with DFT-D3BJ dispersion correction [https://doi.org/10.1063/1.3382344 https://doi.org/10.1002/jcc.21759]. During geometry optimization we used the valence triple-ζ basis set def-TZVP [https://doi.org/10.1039/B508541A] for all atoms. To refine the computed orbital energy, single point calculations were performed using the range-separated hybrid functional ωB97M-V [https://doi.org/10.1063/1.4952647] and the def2-TZVPP [https://doi.org/10.1039/B508541A] basis set. Electrostatic potential figures were generated using Multiwfn [https://doi.org/10.1002/jcc.22885 https://doi.org/10.1063/5.0216272 https://doi.org/10.1039/D1CP02805G] to produce cube files, and visualised with VMD [https://doi.org/10.1016/0263-7855(96)00018-5].